Parameterization of particle formation rates in distinct atmospheric environments

Xinyang Li[1,*], Tuomo Nieminen[1,2], Rima Baalbaki[1,3], Putian Zhou[1], Pauli Paasonen[1], Risto Makkonen[4], Martha A. Zaidan[1,5], Nina Sarnela[1], Chao Yan[1,6], Tuija Jokinen[1,3], Imre Salma[7], Máté Vörösmarty[8], Tuukka Petäjä[1], Veli-Matti Kerminen[1], Markku Kulmala[1,6], Lubna Dada[1,9,*]

[1] Institute for Atmospheric and Earth System Research (INAR), University of Helsinki, Helsinki, 00560, Finland

[2] Department of Physics, Faculty of Science, University of Helsinki, Helsinki, Finland

[3] Climate & Atmosphere Research Centre (CARE-C), Cyprus Institute, P.O. Box 27456, Nicosia, 1645, Cyprus

[4] Hevesy Climate System Research, Finnish Meteorological Institute, P.O. Box 503, 00101 Helsinki, Finland

[5] Department of Computer Science, University of Helsinki, Helsinki, 00560, Finland

[6] Joint International Research Laboratory of Atmospheric and Earth System Sciences, School of Atmospheric Sciences, Nanjing University, Nanjing, 210023, China

[7] Institute of Chemistry, Eötvös Loránd University, Budapest, Hungary

[8] Hevesy György Ph.D. School of Chemistry, Eötvös Loránd University, Budapest, Hungary

[9] PSI Center for Energy and Environmental Sciences, Villigen PSI, Switzerland

Correspondence to: Xinyang Li (xinyang.li@helsinki.fi), Lubna Dada (lubna.dada@helsinki.fi)

Abstract. Atmospheric particle formation rate (J) is one of the key characteristics in new particle formation (NPF) processes worldwide. It is related to the development of ultrafine particle growth to cloud condensation nuclei (CCN) and, hence, to Earth radiative forcing in global models, which helps us to better understand the impact of NPF on cloud properties and climate change. In this work, we parameterized four semi-empirical J models for 5 nm atmospheric particles using field measurements obtained from distinct environments that varied from clean to heavily polluted regions and from tropical to polar regions. The models rely primarily on sulfuric acid as a condensing vapor, condensation sink to account for the vapor loss, and relative humidity for meteorological contribution to J. However, the dependencies between J, condensation sink, and relative humidity are affected by their interlinked relations to sources and sinks of other condensable vapors than sulfuric acid and the potential traffic emissions to the observed size range. The parameterization results showed that our models were able to produce plausible predictions for boreal forest environments, heavily polluted environments, and biogenic environments with high relative humidity. We further tested the models in the global simulation module Tracer Model 5 (TM5, massive parallel version) to simulate particle number size distribution across 14 global atmospheric

Commented [XL1]: Modification for RC1, Comment 4,5,6 combined. Part 5/6.

measurement sites. The simulated results showed satisfactory predictions on particle number concentrations for all the tested environments, with significant improvement in the nucleation mode, and better prediction accuracy for Aitken and accumulation modes compared to the binary sulfuric acid-organic vapor model in Riccobono (2014). Our study has successfully provided powerful tools to predict J_5 on a global scale across various environment types using the most essential and more accessible variables involved in the NPF processes. Essentially, this work reinforces the necessity for global research into the investigation of environment-oriented meteorology-involved NPF processes.

1 Introduction

Atmospheric new particle formation (NPF) is a natural phenomenon observed globally (Bousiotis et al., 2021; Brean et al., 2023; Gordon et al., 2017; Kerminen et al., 2018; Nieminen et al., 2018). As particles form and grow on regional scales, they can reach large enough sizes at which they can act as cloud condensation nuclei (CCN) for water vapor to condense onto when forming clouds. This process affects cloud properties (Roldin et al., 2011; Sanchez et al., 2016; Spracklen et al., 2008) and ultimately the global climate depending on the particle numbers, sizes and their chemical compositions (Bellouin et al., 2020; Calvo et al., 2013; Uno et al., 2020). Particle formation rate (J) is an essential parameter describing the NPF intensity, which is often utilized to represent NPF in global models to simulate the effect of NPF on cloud properties and radiative forcing on Earth. To derive a representative parametrization of J for global simulation, we require a broad understanding of NPF in different environments temporally and spatially. That being the case, the atmospheric measurements of both particle number size distributions and NPF precursor vapors are essential to obtain for the atmospheric observations and model developments.

The NPF processes have been investigated and parameterized based on particle formation mechanism theories (Chang et al., 2009; Kulmala et al., 2001; Lehtinen and Kulmala, 2003), field measurements from specific environments, such as pristine boreal forests (Kulmala et al., 2001; Nieminen et al., 2011; Paasonen et al., 2010), urban cities (Salma et al., 2011, 2016, 2021; Salma and Németh, 2019; Zhang et al., 2010), rural area (Lee et al., 2019; Yli-Juuti et al., 2009), marine environment (Zhang et al., 2010), and also chamber experiments (Kirkby et al., 2011; Lehtipalo et al., 2018). In addition to neutral particle formation mechanisms, the ion-induced nucleation is also covered in J parameterizations (e.g. Nieminen et al., 2011; Määttänen et al., 2018). The existing literature primarily focused on the particle activation and survival of nucleation mode particles down to 1.5 nm, involving complex micro-physics of aerosol particles, such as nanometer clusters production, losses due to clusters

coagulation and growth (Bousiotis et al., 2021; Chu et al., 2019; Kerminen et al., 2018; Nieminen et al., 2018). Furthermore, distinct effects on particle formation rates influenced by the same factors were seen under comparable environmental settings. However, these environment-specific models typically have limited application for global simulation implementations that encompass the diverse atmospheric conditions on Earth.

To simulate particle formation rates, one usually starts from the nucleation mode size range. Global modelers have been facing great challenges in simulating nucleation mode particles because large-scale models have limited capabilities in treating the complicated aerosol dynamics taking place in the sub-5 nm particle size range. The formation rate at 5 nm is shown to be important because after sizes of about a few nm in diameter, particle growth rates show relatively limited variability in different environments (Kulmala et al., 2022a, b, 2023). In addition, we currently do not have a good enough theoretical understanding on the processes dictating particle growth rates at the smallest sizes, nor the survival of such particles from coagulation scavenging (e.g. Cai et al., 2022; Tuovinen et al., 2022; Marten et al., 2022).

The essential parameters for *J* parameterizations should include at least one type of precursor vapor, some may also cover meteorological parameters, and the sinks for vapors and particles. For instance, sulfuric acid (H_2SO_4) as the most known precursor vapor plays a critical role in particle formation and growth processes due to its low volatility (Kulmala et al., 2004; Myllys et al., 2019). In the earlier parameterizations of NPF mechanism, *J* correlated (linearly or squared) with H_2SO_4 concentrations in various environments (Paasonen et al., 2010). In terms of meteorology, air temperature (*T*), relative humidity (RH), global solar radiation (GRad), wind speed (WS), and wind direction influence the particle formation rates in certain environments as well (Laarne et al., 2022; Salma et al., 2021; Zaidan et al., 2018). The variation of *T* can influence the precursor vapor formation and stability of NPF processes: a higher *T* can enhance the biogenic emissions that participate in particle formation in a boreal forest (Dada et al., 2017; Nieminen et al., 2015), while a lower *T* favored the H_2SO_4-amine clusters stability in a megacity (Deng et al., 2020). RH can impact the precursor vapor formations as well as the aerosol formation rates (Ding et al., 2021; Hellmuth, 2006). The variation of RH is dependent upon *T* so that the rise of *T* during daytime increases the planetary boundary layer height (PBLH), which in turn dilutes the air mixture and decreases the RH (Liu et al., 2018) as well as particle number concentrations (Mazon et al., 2016) in the atmosphere. For condensable vapor loss, we usually include the term condensation sink (CS), which describes the loss rate of condensable vapors to aerosol particles, and it typically declines before an NPF event starts. H_2SO_4 concentrations, on the other hand, increase due to the reduction in CS, which means that the condensable vapors are not lost onto the aerosol particles as efficiently as they would be at greater CS values (Hellmuth, 2006; Kulmala et al., 2012).

In general, the developed *J* models underestimate the observed particle number concentration, which may be attributed to NPF schemes being poorly represented in these models. Many *J* parameterization works were conducted focusing on the formation mechanisms from sulfuric acid (Paasonen et al., 2010), sulfuric acid-water (Määttänen et al., 2018), sulfuric acid-ammonia (Glasoe et al., 2015), and sulfuric acid-organic vapor (Paasonen et al., 2010; Riccobono et al., 2014). However, some models are likely applicable only to certain types of environment, or they primarily cover the microphysics of the particle nucleation at sub-3 nm range, where the nucleated clusters face higher instability due to the higher evaporation rates than condensation rates (Deng et al., 2021; Wang et al., 2011). Bergman (2022) attempted an organic-vapor-based NPF scheme in addition to the commonly used binary water-sulfuric-acid-based scheme to simulate global particle formation and number concentrations. This scheme improved the simulated number concentrations across the observation stations, although they were still underestimated compared to the observations, suggesting that the parameterization of early growth of particles to 5 nm diameter still requires improvement.

To predict the particle formation rate at 5 nm originating from NPF and subsequent growth, as well as to understand and predict the climatic impacts caused by NPF and initial growth in global scale, we parameterize particle formation rates (J) at 5 nm using combined measurement data from six different environments: Hyytiälä (boreal forest close to rural environment, Finland), Beijing (megacity, China), Värriö (remote boreal forest, Finland), Budapest (urban, Hungary), Agia Marina Xyliatos (rural, Cyprus) and Manacapuru (Amazonian basin, Brazil). The parameterizations of *J* were based on the analysis of atmospheric particle number-size distributions. Sulfuric acid concentrations, RH and CS are the main input variables in the parameterization models. By including information from various types of environments, we will be able to demonstrate whether our models can adequately explain the formation rate of 5 nm particles on a wider environmental scale. The parameterized models are then incorporated into EC-Earth models to simulate particle formation rates in the global scale (the European community Earth-System Model, EC-Earth, chemistry transport model TM5: Tracer Model 5, version TM5-chem-v3.0, details in supplement) (Huijnen et al., 2010).

This work aims to provide an effective tool for global particle formation rate estimations. Our parameterizations have three main features: (1) the number of inputs is limited to be the most essential parameters involved in NPF process, (2) they do not involve complex microphysics at particles smaller than 5 nm, and (3) they cover a wide range of environment types. These features will enhance the applicability of the parameterizations for the purpose of global model application.

2 Measurement locations and instrumentation

This study includes measurements from six different sites representing different environmental conditions. A summary for all locations and the instrumentation used is given in Table S1. Figure 1 shows the map of the measurement sites included in this study.

2.1 Measurement sites

2.1.1 Rural boreal forest environment: Hyytiälä, Finland

The measurement data were obtained from the SMEAR II-station (Station for Measuring Ecosystem–Atmosphere Relations), situated in a Scots pine (*Pinus sylvestris*) forest in Hyytiälä (61.1 N, 24.17 E; 181 m (a.s.l).; Hari and Kulmala, 2005), southern Finland. This measurement site is described as having a rural regional background with minimal anthropogenic emission. Hyytiälä data covered the period from 21 March 2016 to 18 August 2019.

2.1.2 Remote sub-arctic boreal forest: Värriö, Finland

The SMEAR I measurement station (67°45′31° N, 29°36′41° E, 390 m a.s.l.) was built on the top of Kotovaara hill located in north-eastern Finland. Similar to Hyytiälä, the site is also a rural background covered mainly by Scots pine (*Pinus sylvestris*) forest located at the north side of the Värriö fell range. However, it is affected by potential polluted airmass that comes from Kola peninsula rather than local industrial pollutants. A detailed description of SMEAR I station can be found in (Kyrö et al., 2014). The data used from Värriö were from 5 April to 13 August 2019.

2.1.3 Polluted megacity: Beijing, China

In Beijing, the measurements were performed at the west campus of the Beijing University of Chemical Technology (BUCT, 39.94° N, 116.30° E, 20 m a.s.l.). The sampling took place from outside the window on the 5th floor of the university building close to a street with busy traffic. For more details on the description of BUCT measurement site, see Liu et al., 2020. The data were available from 29 May 2018 to 3 April 2019.

2.1.4 Urban site: Budapest, Hungary

The measurements took place at the Budapest platform for Aerosol Research and Training (BpART) Laboratory (47.47° N, 19.06° E; 115 m a.s.l.) of the Eötvös Loránd University situated on the bank of the river Danube. The site represents a mixed average atmosphere of the city center (Salma et al., 2016). The data were obtained from 22 March to 17 April 2018.

2.1.5 Mediterranean rural site: Agia Marina, Cyprus

The measurements were conducted at the Agia Marina Xyliatou (AMX) station (35.03° N, 33.05° E; 532 m a.s.l.) of the Cyprus Atmospheric Observatory (CAO). The site represents a rural background location situated at the foothills of Troodos mountains, with agriculture land in the vicinity. The data were obtained between 22 February and 3 March 2018. For more details about the site, see e.g. Baalbaki et al., (2021).

2.1.6 Amazonian basin: Manacapuru, Brazil

The Manacupuru measurement site was in a pastureland 70 km west of Manaus, Brazil, in central Amazonia. This site receives airmass from various resources, including rural, biogenic and anthropogenic from the nearby municipality (Manaus). The trace gases and meteorological measurements were performed during the GoAmazon2014/5 campaign at the T3 site (3.2133◦ S, 60.5987◦ W 50 m a.s.l.), 10 km northeast of Manacapuru, Brazil (Martin et al., 2016; Schiro et al., 2018). A more detailed description of the measurement site can be found in (Myers et al., 2022). The data covered the time period from 22 August 2014 to 9 October 2014.

2.2 Instrumentation

2.2.1 Sulfuric acid measurements and proxies

H_2SO_4 concentrations were measured at all sites, except for the Amazonian basin, using a Chemical Ionization Atmospheric Pressure interface Time-of-Flight spectrometer (CI-APi-ToF) (Eisele and Tanner, 1993; Jokinen et al., 2012) with NO_3^- as the reagent ion and analyzed using tofTools package based on MATLAB software (Junninen et al., 2010). In the Amazonian basin, H_2SO_4 concentrations were measured using a selected ion chemical ionization mass spectrometer (SICIMS), see Myers et al., (2022) for more details. The H_2SO_4 concentration measurements were taken from different levels ranging from ground level up to 35 meters above ground level. The CI-APi-ToFs were calibrated uniformly before the measurement in each location following the technique described

by (Kürten et al., 2012), except for the Amazonian basin where the selected ion chemical ionization mass spectrometer (SICIMS) was calibrated following the scheme described in Mauldin III et al. (1998).

To increase the applicability of our derived parameterization, H_2SO_4 proxy data from Hyytiälä and Beijing were included as an additional testing data set. The proxy data were calculated using the proxy specific for the boreal forest environment and polluted megacity developed by Dada et al., (2020). For Hyytiälä, the sulfuric acid proxy data ranged from 22 August to 25 December 2016, and 8 March 2018 to 26 February 2019, denoted as Hyytiälä$_{SAprx}$; For Beijing, the time period was from 15 March to 3 April 2019, denoted as Beijing$_{SAprx}$. The subscript "SAprx" (SA as in sulfuric acid) in Hyytiälä$_{SAprx}$ and Beijing$_{SAprx}$ indicates that the datasets utilize H_2SO_4 concentration from proxies as input for the testing dataset.

2.2.2 Particle number size distribution

The particle number size distribution (PNSD) measurements were obtained from different types of setups in each site. Hyytiälä: twin-Differential Mobility Particle Sizers (DMPS; Aalto et al., 2001); Värriö: Differential Mobility Particle Sizers (DMPS) (Jokinen et al., 2022); Beijing: Particle Size Distribution (PSD) system with a nano-Differencial Mobility Analyzer (DMA) and an Aerodynamic Particle Sizer (APS) (Zhou et al., 2021); Budapest: flow-switching-type DMPS (6 – 1000 nm; Salma et al., 2016); Cyprus: Neutral cluster and Air Ion Spectrometer (NAIS) and Scanning Mobility Particle Sizer (SMPS; Baalbaki et al., 2021); Amazonian basin: the measurements were conducted using SMPS (10 – 1000 nm). It is important to note that we do not aim to compare the PNSD measurements from all the chosen sites. Instead, the PNSD measurements were used to calculate the formation rates based on changes in particle number concentrations under local conditions.

2.2.3 Meteorological variable

The meteorological variables included in this study are relative humidity (RH, %) and ambient temperature (*T*, ºC). In Hyytiälä, RH and *T* were measured at 16.8 m using Rotronic MP102H RH sensor (Rotronic Hygromet MP102H with Hygroclip HC2–S3, Rotronic AG, Bassersdorf, Switzerland); In Värriö, RH and *T* were measured by a Rotronic MP106A captive sensor; In Beijing, RH and *T* were monitored by Vaisala weather station (AWS310); In Budapest, RH and *T* were monitored using Vaisala HMP45D temperature and humidity probe, and Vaisala WAV15A anemometer located on on-site of the BpART Lab; In Cyprus, RH and *T* were measured by a meteorological station in a nearby village (35.01◦ N, 33.05◦ E), 2.85 km away from the measurement site; In Amazonian basin, RH and *T* were measured at the Atmospheric Radiation Measurement (ARM) user facility.

2.3 Data analysis

2.3.1 Calculation of particle formation rates

To develop more inclusive and generalized models, the parameterization included data from both NPF event days and non-event days. This approach recognizes that the production of atmospheric secondary particles from non-NPF events (days with no apparent particle growth) is becoming more significant in a world with growing anthropogenic influence (Kulmala et al., 2022a). Such a measure would increase the applicability of our models on a global scale.

The observed particle formation rates (J_5) at 5 nm were calculated from the measured PNSD according to Equation 1 (Kulmala et al., 2012).

$$J_{d_p} = \frac{dN_{d_p}}{dt} + CoagS_{d_p} * N_{d_p} + \frac{GR}{\Delta d_p} * N_{d_p} \quad \text{(Eq. 1)}$$

The first term dN_{dp}/dt is the change in concentration in the size bin, 5–9 nm. Ideally, this term, as well as the concentration of particles within the size range, N_{dp}, in the following terms, are associated with the growth of particles formed by atmospheric NPF past 5 nm; however, especially in traffic-related environments, they may also have an unknown contribution by direct particle emissions to this respective size range (Okuljar et al., 2021; Rönkkö et al., 2017). The second term $CoagS_{dp}$ is the coagulation sink, which describes the 5-9 nm particle losses due to coagulation with larger particles calculated from the PNSD at each measurement site (Kulmala et al., 2012). The third term describes the loss of particles due to their growth out of the size bin. Here, we calculated the growth rates (GR) of 5–9 nm particles using the maximum concentration method (Kulmala et al., 2012) for days classified as NPF event days as described by Dal Maso et al., (2005). The GR for non-event days was approximated using the normalized PNSD from the sum of non-NPF events at each site. Such approximation is validated for several locations as a 'quiet NPF' occurs with the similar GR as that on NPF event days (Kulmala et al., 2022a).

Commented [XL2]: Additional text considering the overall Referee Comments.

2.3.2 Extrapolation of particle formation rates

For Budapest and the Manacapuru (Amazonian basin), the particle formation rates were calculated from PNSD measurements at 6 nm and 10 nm, respectively. Therefore, we obtained J_5 by extrapolating from J_6 and J_{10} respectively. The J_5 extrapolation followed the analytical formula derived by Kerminen and Kulmala (2002). We extrapolated J_5 from J_6 for Budapest. For Manacapuru, the extrapolations were done separately for J_{10} (wet season) and J_{14} (dry season), due to the particle size limit of the measurement instrument.

2.3.3 Condensation and coagulation sink (CS and CoagS)

The CS and CoagS were calculated from the measured PNSD data for each site using the method proposed by Kulmala et al., (2012). To ensure the comparability between all locations, both CS and CoagS were calculated without the correction for hygroscopic growth. There are several ways to determine the hygroscopic growth factors in CS and CoagS calculations. Laakso et al., (2004) developed parameterizations for Hyytiälä solely based on the meteorological conditions and the aerosol composition in Hyytiälä, which results in the inapplicability of that method to other sites. In the Supplementary of Baalbaki et al., (2021), Figure S4 shows the CS with hygroscopic correction is about 1.1 – 1.3 times higher than dry CS, which would result in an overestimation on CS for the case in Cyprus. Petters and Kreidenweis (2007) introduced the single hygroscopicity parameter κ (kappa), which can be derived from Humidified Tandem Differential Mobility Analyzer (HTDMA) or cloud condensation nuclei counter measurements or based on aerosol chemical composition obtained from instruments such as the Aerosol Chemical Speciation Monitor (ACSM) or Aerosol Mass Spectrometers (AMS). In other locations, since organics are typically the dominant component of aerosol mass in continental areas or marine polluted areas (Chen et al., 2022) and are less hygroscopic than inorganics, one can expect an underestimation of CS similar to the one reported in (Baalbaki et al., 2021). As a result, we omitted the hygroscopic growth impact for the chosen measurement sites to harmonize the data composition and the later model analysis.

Commented [XL3]: Additional text for RC1, Comment 1. Part 1/2.

2.3.4 Datasets

The parameterizations were developed using the combined dataset from all six measurement sites in hourly time resolution. Data points were selected considering detection limit of the instruments and therefore, the filters were set to be $J_5 > 1\times10^{-5}$ cm^{-3} s^{-1}, H_2SO_4 concentration $> 5\times10^{3}$ cm^{-3}, RH $\in$ [0,100] % and CS $> 1\times10^{-5}$ s^{-1}. The complete dataset was afterwards randomly resampled into a training set (75% from the complete dataset) and a testing set (25% the rest of the complete dataset) for parameterization. In model testing, we included two additional inputs from H_2SO_4 concentration proxies developed by Dada et al., (2020) from Hyytiälä and Beijing. The detailed number of data points per site are shown in Table 1. The data distribution and comparison of each input variable are displayed in Figure S2, where the overall variations of the input variables across the six sites are distinct in their range and intensity, which pronounces the inclusivity of model training for a wider application in global environments.

3 Parameterization of J_5

3.1 Derivation of parameterization models

We derived the parametrized J_5 based on the input variables (H_2SO_4, RH, CS), which were chosen based on field observations that highlighted their roles in the particle formation mechanism across various environments (Baalbaki et al., 2021; Dada et al., 2020; Kerminen et al., 2018; Myers et al., 2022; Salma et al., 2016, 2021; Yan et al., 2021). It has been discovered that NPF events occur favorably under lower RH, for example in boreal forests (Dada et al., 2018; Yao et al., 2018), Mediterranean regions (Debevec et al., 2018), from CLOUD chamber experiment (Duplissy et al., 2016) and model studies (Hamed et al., 2011). RH was shown to be seasonally related to cloudiness and global radiation, so that a decreasing global radiation can lead to an increased RH and cloudiness within the troposphere (Ruosteenoja and Räisänen, 2013). To reduce the model complexity, we opted to use RH as an indirect indicator of global radiation. A lower CS facilitates the occurrence of NPF events even in contrasting environments with distinct types of condensable vapor. For example, CS is a measure of a sink for anthropogenic vapors in a megacity (Wang et al., 2011) and for biogenic vapors in a clean boreal forest (Dada et al., 2017; Tuovinen et al., 2020), as well as a sink for growing sub-5 nm clusters and particles (Kulmala et al., 2017). When combined with H_2SO_4 as an input variable, the evidently important sink effect of a pre-existing particle population on the ambient H_2SO_4 concentration is implicitly transferred from CS to H_2SO_4 in our parameterization. Indirectly, CS may also be associated, either causally or not, with 1) emissions or sinks of vapors other than H_2SO_4 participation in NPF or particle growth, and 2) primary particle emissions from traffic, which would influence particle formation rates estimated from observations using eq. 1. Furthermore, since we omit the influence of hygroscopic growth of particles on CS, a fraction of real sink effect of CS is implicitly transformed to the variable RH in our parameterization.

We tested with T as an input variable during model derivation and training. However, the modelled results did not show improvement compared to the current parameterization, suggesting that T provided redundant information for describing particle formation in the context of our model's global application.

Other than sulfuric acid, highly oxygenated organic molecules (HOMs) and ammonia (NH_3) have been discovered to play a significant role in particle formation process (Bianchi et al., 2019; Lehtipalo et al., 2018). The possible cluster types may include H_2SO_4-NH_3-H_2O (Yu et al., 2018) and HNO_3-related clusters such as HNO_3-H_2SO_4-NH_3 in the upper tropospheric particle nucleation (Wang et al., 2020, 2022, 2023). Yet, we are unable to include HOM nor NH_3 concentrations owing to limited data availability from the chosen measurement sites. So far, long-term

Commented [XL4]: Additional text for RC1, Comment 1. Part 2/2.

Also for RC2, Comment 2.

Commented [XL5]: Modification for RC2, Comment 6.

measurements (> 1 year) of HOMs, matching the time range covered by other variables, are only available in Hyytiälä from a CI-APi-ToF mass spectrometer. However, this is not the case at other sites, limiting our ability to have simultaneous HOMs data across all environments included in this study. Similarly, the NH_3 concentrations either did not cover the same time period as other variables or were unavailable for the other environments.

3.1.1 Different versions of the parameterization models

The derived model functional forms are as follows:

Model 1 (the baseline model, Eq. 2) presents the simplest particle formation mechanism based solely on the abundance of the precursor vapor H_2SO_4 concentrations in the atmosphere. The coefficient k_1 serves as a scaling coefficient that represents the activation rate of clusters in the presence of H_2SO_4 molecules during cluster formation (Kulmala et al., 2006; Paasonen et al., 2010).

$$J_5 = k_1 \times [H_2SO_4] \quad \text{(Eq. 2)}$$

Model 2 (Eq. 3) introduces RH in addition to model 1 to partially represent the effect of the changing meteorological conditions relating to the global radiation and ambient water vapor content on J_5 in general in different types of environments (Dada et al., 2017; Hamed et al., 2011; Li et al., 2019). The coefficient k_2 serves as a scaling coefficient and shown as the activation efficiency of the nucleated clusters.

$$J_5 = k_2 \times [H_2SO_4] \times RH^{k_{RH}} \quad \text{(Eq. 3)}$$

Model 3 (Eq. 4) includes, in addition to model 2, the factor CS. As discussed above, in our parameterization CS is connected not only to the sink of newly formed particles prior to their growth past 5 nm, but possibly also to sinks or sources of vapors other than H_2SO_4 participating in particle formation and growth and, in polluted environments, to sub-10 nm particle emissions from traffic. The coefficient k_3 serves as a scaling coefficient for the activation and survival efficiency of the nucleated clusters.

$$J_5 = k_3 \times [H_2SO_4] \times RH^{k_{RH}} \times CS^{k_{CS}} \quad \text{(Eq. 4)}$$

Model 4 (Eq. 5), additionally accounts for the formation of H_2SO_4 multimers in the gas phase prior to cluster formation as assumed by the kinetic theory (McMurry and Friedlander, 1979), the coefficient k_{SA} represents the number of H_2SO_4 molecules (2, 3, 4, etc…). Therefore, k_4 in this case is not the activation coefficient anymore but includes both the collision frequency and the probability of a stable particle formation after the collision (Sihto et al., 2006; Weber et al., 1996).

$$J_5 = k_4 \times [H_2SO_4]^{k_{SA}} \times RH^{k_{RH}} \times CS^{k_{CS}} \quad \text{(Eq. 5)}$$

Commented [XL6]: Additional text considering the overall Referee Comments.

3.2 Model training results

To derive a parametrized J_5 based on precursor and other input variables from the training dataset, we used the "*fmincon*" optimization algorithm in MATLAB to retrieve the values of each coefficient (k_1-k_4, k_{SA}, k_{RH} and k_{CS}) from the training datset. The coefficients obtained for each of the models can be found in Table 2. The derived models with the optimized coefficients were applied to the testing datasets and compared with the observed J_5 and the parametrized J_5. We evaluated the performance of each model based on the data distribution, the resulting deviation from observation and its uncertainty. To maintain the global model's simplicity, the parameterization covered both daytime and night-time data for all sites in all models.

Figure S3 presents the measured to modelled J_5 from model 1-4 using training dataset from six measurement sites, including the slopes and coefficient of determination (R^2). Overall, by comparing model 1 (Fig. S3a) and model 2 (Fig. S3b), we observed an improvement in the model performance with the inclusion of RH. The R^2 value improved from 0.28 to 0.44, and the slope increased from 0.29 to 0.56. This observation confirmed the importance of considering meteorological impact when parameterizing J_5. By further including CS in model 3, the model improved further (Fig. S3c), with the R^2 increasing from 0.44 to 0.49, and the slope from 0.56 to 0.62. To further introduce the kinetic theory and the formation of H_2SO_4 dimers and other multimers, we added an exponent over H_2SO_4 in model 4 (Fig. S3d). This addition showed a further improved correlation and slope between the measured or modeled data for the training datasets (R^2 = 0.57, slope = 0.76). In subsequent testing, model 4 generally outperformed the other models (see section 4, Fig. 2).

3.3 Model evaluations

3.3.1 MAE and RMSE

We computed the mean absolute errors (MAE), root mean square errors (RMSE) for each model using the testing dataset to gain a better understanding of the models' performance. The numerical values of MAE and RMSE are given in Table S3.

The MAE calculation equation is as follows:

$$MAE = \frac{1}{n}\sum_{i=1}^{n}|y_i - \hat{y}_i| \qquad \text{(Eq. 6)}$$

where n is the number of data points (here it is the total number of data points from testing set, see Table 1), y_i is the observed value, and $\hat{y}_i$ denotes the predicted value. MAE measures the accuracy of models' prediction power, by quantifying the average magnitude of errors between observed and predicted values (Chai and Draxler, 2014). A lower model error is manifested by a lower MAE value.

The RMSE is calculated as the square root of the difference between the measured (y_i) and predicted ($\hat{y}_i$) J_5 values normalized by the number of data points.

$$RMSE = \sqrt{\frac{1}{n}\sum_{i=1}^{n}(y_i - \hat{y}_i)^2} \quad \text{(Eq. 7)}$$

RMSE also measures the average magnitude of errors of models. However unlike MAE, RMSE squares the errors giving greater weight to larger errors and penalizing them more heavily (Chai and Draxler, 2014). Therefore, RMSE values reveal whether the models' performances are highly influenced by large prediction errors Similar to MAE, lower RMSE values indicate better model performance.

Figure S4 (upper panel) depicts a declining trend of the overall MAE from models 1 to 4 (Eqs. 2-5). For the environmental types investigated in this study, the MAE values of the four models from all sites are lower than 1, indicating that the mean differences on the magnitude for J_5 are minor when utilizing the parameter settings from our models. However, Budapest stands out due to the apparent higher MAE, potentially highlighting the distinct NPF mechanism in Budapest compared to the other sites as well as the seasonal limitations on its data (spring 2018 only).

The RMSE values increased as more parameters were added into the model, peaking for model 3 (Fig. S4, lower panel), even though model 3 can predict J_5 for multiple types of environments on a satisfactory level. We can see that from model 1 to model 2, the inclusion of RH increased the model errors more compared to the addition of CS from model 2 to model 3. However, the RMSE values dropped significantly when H_2SO_4 was allowed to vary with an exponent k_{SA} in model 4 in the presence of both RH and CS.

Based on the results summarized above, models 3 and 4 (Eqs. 4 & 5) seem to be the most promising for global J_5 prediction among all model types owing to their low MAE values. However, the lower RMSE for model 4 showed its outperformance to model 3.

3.3.2 Akaike Information Criterion

The Akaike Information Criterion (AIC) is a statistical measure that helps to evaluate the goodness-of-fit of a statistical model. We use AIC as an evaluation tool because it can evaluate models with different number of parameters and complexities, ensuring a balanced assessment. Eventually, it allows us to select the model with the best balance between the model complexity and goodness-of-fit. The parameters used to calculate the AIC for each site are shown in Tables S4-S6. A lower AIC score indicates a superior goodness-of-fit and a lower tendency for model overfitting. The relative likelihood term (L, $L = e^{(AICmin-AICi)/2}$), calculated from AIC scores, reflects the likelihood that the *i*th model minimizes information loss as compared to the model with the lowest AIC. A relative likelihood of 1 suggests that the model outstands other models in minimizing information loss. For boreal forest environments (Table. S4), and urban environments (Table. S5), both models 1 and 4 minimized information loss the most. For rural regions, model 4 (Eq. 5) performs the best (Table. S6). Compared to the baseline model (model 1, Eq. 2), we find that H_2SO_4 is a more powerful parameter than RH or CS in all environments. However, in Manacapuru, including RH and CS shows clearly an improved predictive accuracy in model 4 (Eq. 5).

4 Results and discussion

4.1 Parameterization testing results

The scatterplots (Fig. 2) demonstrate the overall performance of the parameterizations from the 4 models (Eqs. 2-5) using the testing dataset. The overall and site-specific Pearson's coefficients, slopes from robust linear fit between the measured and modelled J_5, as well as the number of data points from the testing dataset, can be found in Table 3. Overall, r increased significantly for model 2 and 3 (Fig. 2b & 2c, $r = 0.69$, $r = 0.71$) compared to model 1 (Fig. 2a, $r = 0.55$) as we include relative humidity and condensation sink as model parameters. Model 4 provides the best linear fit results, implying that the model can predict an overall reliable estimation on J_5 in all the investigated environment types (Fig. 2d, $r = 0.78$). It is notable that with the combined data sets, the condensation sink receives a positive exponent in models 3 and 4 ($k_{CS} = 0.56$ and 0.67, respectively), likely due to its association with concentrations of other condensable vapors than H_2SO_4 and traffic emissions.

Commented [XL7]: Modification for RC1, Comment 4,5,6 combined. Part 2/6.

4.1.1 Boreal forests: Hyytiälä and Värriö

Given the boreal forest background, Hyytiälä and Värriö exhibited comparable variations in the distribution of modelled J_5 values from the four model types. As shown in Figure 3, model 3 ((a3), (b3), (c3)) and model 4 ((a4), (b4), (c4)) illustrated a more centered data distribution between the modelled and measured J_5, which demonstrates a potential favoring of NPF under low RH conditions, likely associated with increased global radiation for the boreal forest environment (Dada et al., 2018; Hamed et al., 2011) and lower sinks for vapors and growing sub-5 nm particles (see Section 3.1). Notice that the mean H_2SO_4 concentration in Värriö is about twice as high as that in Hyytiälä, opposite to CS which is clearly lower in Värriö (Table S2). The low CS in Värriö compared with Hyytiälä is primarily due to the lower emission rate of the regional precursor vapors (e.g. Tunved et al., 2006), leading also to the lower observed NPF event frequencies (Kyrö et al., 2014; Neefjes et al., 2022). We must note that the Hyytiälä data spanned three years, containing more data points for model training, whereas the Värriö data only covered the period from April to August 2019, excluding the entire cold season when H_2SO_4 concentrations are significantly lower than those during the warm season (Jokinen et al., 2022). As a result, our model 3 (Fig. 3(a3), (b3), (c3)) and 4 (Fig. 3(a4), (b4), (c4)) can predict J_5 for boreal forest environment on a satisfactory level, including the possibility to use the estimated H_2SO_4 concentration from proxies as input. Nevertheless, limitations regarding precursor vapor production rate could potentially influence the prediction accuracy.

4.1.2 Urban-influenced: Beijing and Budapest

In anthropogenic emissions dominated region, such as Beijing, the measured and modelled J_5 are well aligned around the 1:1 line using model 3 (Fig. 3(d3), (e3), (f3)), and model 4 (Fig. 3 (d4), (e4), (f4)). In Beijing, a polluted megacity, the dominating precursor type has been found to be H_2SO_4–amine clusters (Cai et al., 2021). As expected, the testing result showed dramatic underestimations for Beijing using model 1 with only H_2SO_4 concentrations considered (Fig. 3(d1)), whereas models 2 (Fig. 3(d2)) and 3 (Fig. 3(d3)) yielded clearly enhanced J_5 predictions, with relatively minor differences between models 2 and 3. These features are consistent with the fact that in addition to H_2SO_4, also other vapors are import to NPF and sub-5 nm particle growth in Beijing, and demonstrate that RH and CS in our parameterization together determine in a complicated way the sources and sinks of these vapors, the survival probability of sub-5 nm particles, and the potential emissions of sub-10 nm primary particles from traffic. This study did not include amine-related compounds in the formulas because the lack of measured NH_3 data makes the parallel comparisons difficult among the chosen sites for model training.

Commented [XL8]: Modification for RC1, Comment 3.

Also for RC2, Comment 4.

Commented [XL9]: Modification for RC1, Comment 4,5,6 combined. Part 1/6.

For Budapest, a large European city, the underestimates in modelled J_5 are not as much improved as they were for Beijing when including RH or CS in the parameterization, which is indicative of distinct particle formation pathways between Beijing and Budapest, even though both sites represent urban background environments. On one hand, it is worth noting that including RH (model 2, Eq. 3) resulted in a decrease in the correlation coefficients between the measured and modelled J_5 in Budapest from 0.54 to 0.46 (Table 3). This suggests that the role of RH in the NPF process in Budapest is less significant than other chosen inputs, despite previous indications that high RH levels have a strong potential to suppress NPF during non-event days in Budapest (Salma et al., 2021), even though the RH values in Budapest were considerably higher than those in Beijing (Table S2). On the other hand, including CS (model 3, Eq. 4) in addition to RH (model 2, Eq. 3) leads to an increase in the correlation coefficients between the measured and modelled J_5 from 0.46 to 0.61 (Table 3). We used both NPF and non-NPF days during model training even though it was found that CS was 50% lower during non-NPF events in Budapest than the values during NPF events (Salma et al., 2016). As a result, it is difficult to determine if the model's performance gain was entirely brought on by the addition of CS. Otherwise, the results are all in line with the earlier indirect evidence that chemical species other than H_2SO_4 influence the particle growth and possibly NPF process in Budapest (Salma and Németh, 2019). If one considers additional vapors other than H_2SO_4 for Budapest alone for J parameterization, one could include oxidation products of VOCs originating from either urban vegetation emissions or traffic emissions. For example, isoprene oxidation products can be used to describe the inhibiting effect on NPF (Heinritzi et al., 2020; Kiendler-Scharr et al., 2009), while monoterpene oxidation products could enhance sub-3 nm particle growth (Kulmala et al., 2013).

Commented [XL10]: Addition text for RC2, Comment 7.

Based on the testing results, model 3 is more likely to predict a more accurate J_5 for Beijing based on the highest AIC ratio (except for 1), while model 1 predicts better for Budapest. Notice the fact that J_5 showed distinct levels of measured J_5 dependence with RH and CS in Beijing and Budapest (J_5 and RH: Beijing: $r = -0.21$, Budapest: $r = -0.1$; J_5 and CS: Beijing: $r = -0.02$, Budapest: $r = 0.57$, Fig. S1).

4.1.3 Mediterranean rural site: Agia Marina, Cyprus

For Cyprus, it appears that meteorology and condensation sink terms have only minor effects on the formation of 5 nm particles in such rural environment under the influence of marine vapors when comparing the results from testing dataset across models (Fig. 3g). However, including RH improves slightly the correlation between the modelled and measured J_5 as seen in model 2 (r rises from 0.42 to 0.49, Table 3). The reduced values of r in model 3 (Eq. 4) indicate a somewhat reversed impact of CS on J_5, which requires additional examination as J_5 and CS are

weakly correlated (r = 0.03, Fig. S1). The H_2SO_4 concentration showed a low contribution to J_5 with the exponent being less than 1 in model 4 (Table 3), which led to a more underestimated modelled J_5 comparing to model 1 (Fig. 3(g1), (g4)). This could be an indication that potentially other anthropogenic, biogenic or marine compounds are of greater contribution to the particle formation processes in Cyprus than H_2SO_4 (Debevec et al., 2018). Owing to the orographic conditions, the air mass types approaching to the Cyprus measurement site are mixed, including the ones from North Africa, Marine, Europe, and northwest/southwest Asia. This results in the Mediterranean atmosphere in Agia Marina containing various vapors that could influence NPF. The potential key contributors could include oxidation products of dimethyl sulfide (DMS) originating from ocean plankton emissions (Rosati et al., 2021), iodine oxidation products like HIO_3 (He et al., 2021), the stabilizing agent NH_3 (Jiang and Xia, 2017; Lan et al., 2021; Lehtipalo et al., 2018; Yu et al., 2018), and oxidation products of VOCs from the surrounding pines forests and oaks under favorable meteorological conditions (Debevec et al., 2018).

Commented [XL11]: Addition text for RC2, Comment 8.

We should note that the measurements in Cyprus covered only two weeks in springtime, which limited our quantitative observations in model training for other seasons compared to sites with long-term measurements. Based on the findings above, model 1 seems to be the most suitable functional form for the prediction of J_5 in Cyprus.

4.1.4 Amazonian basin: Manacapuru, Brazil

The measured and modelled values of J_5 from the Manacapuru site scatter around the 1:1 line in all the models (Fig. 3). Previous studies reported high RH levels year-round in the measurement site near Manacapuru (Myers et al., 2022; Zhao et al., 2022), which is expected to suppress NPF frequency and to lead to lower formation rates. We observed such suppression effect when taking RH into account as shown by the increased correlation coefficients from 0.004 to 0.19 (Table 3). Studies from Manacapuru suggested that the epoxide vapors could be a potential precursor vapor in particle formation because of anthropogenic influences (Paulot et al., 2009), while Xu et al., (2014) suggested the presence of epoxide vapors can enhance particle nucleation when RH levels increase. We did not observe apparent improved model performance in model 3 when CS is included, as r remained almost unchanged compared to model 2 (Table 3). One factor to consider is that we did not apply hygroscopic growth factor when calculating CS for Manacapuru to maintain the consistency of the training dataset. However, the impact of RH on CS, particularly on the actual particle surface area available for H_2SO_4 uptake, seems to be significant for high RH environments like Manacapuru (Myers et al., 2022). Another assumption could be that even with the high CS, it is still low enough to allow sufficient precursor vapors contributing to NPF processes.

These current findings provide evidence for H_2SO_4 being an effective enough precursor for the particle formation at 5 nm in the atmosphere of Manacapuru (model 1, Fig 3(h1)). However, the RH stabilization effect on H_2SO_4 is not exerted necessarily, as RH remains at high values at around 89 ±13 % despite whether it is measured during wet season or dry season (Myers et al., 2022). With these observations, model 1 with a focus on the H_2SO_4 concentrations manages to predict J_5 well for biogenic vapor dominated environment like Manacapuru.

Commented [XL12]: Modification for RC1, Comment 8.

5 Tracer model 5 simulation

We simulated the particle number size distribution (PNSD) in EC-Earth global chemical transport model TM5-MP (Tracer Model 5, Massively Parallel version, details in supplement) by applying it with our J_5 model 1 and 4. Together, we compared our simulation results with the acid-organic binary homogeneous nucleation model from Riccobono et al., (2014):

$$J_{\text{Riccobono}} = k_m \times [H_2SO_4]^p \times [\text{BioOxOrg}]^q \quad , \qquad \text{(Eq. 8)}$$

where $k_m = 3.27 \times 10^{-21}$ cm^6 s^{-1}, p = 2 and q = 1.

The details of the 14 tested measurement stations are shown in Table S7. Note that the data from these 14 stations are independent from any training or testing datasets used in the previous sections of this paper. Here, we essentially compared the simulated and measured PNSD in three particle modes (nucleation, Aitken, accumulation) from the entire year 2018 to assess the simulation accuracy among global environments.

Figure 4 shows the comparisons of PNSD between the on-site measurements and the TM5-MP simulations. For biogenic environments, simulations using model 4 shows the closest particle number size distribution to the measured ones particularly in Aitken mode particles, promoting the sulfuric acid-based nucleation mechanism involving the source-sink-meteorology even for environment dominated by biogenic vapors. For the Arctic region, model 4 simulated particle concentrations are overall overestimated, while model 1 simulation shows better alignment of particle number concentrations around the Aitken mode. This might indicate that the nucleation process has a lower dependence on the variations of meteorology than we expected. For coastal environments, even though Utö (Baltic Sea Island) and La Réunion (southern hemisphere island) are located at different hemispheres and also have different geographical settings, the nucleation mechanisms from models 1 and 4 both show similar predictions on particle concentrations across particle modes, with larger underestimation in the accumulation mode for model 1. This once again validates the source-sink-meteorology mechanism in model 4. By observing the ratio between the simulated and measured particle number concentrations, we can quickly see that the sulfuric acid-based particle formation mechanisms with (model 4) or without (model 1) meteorology inputs have successfully

narrowed the gap between the simulations and observations across all particle modes, with significant improvements for the nucleation mode (Fig. 5). The "Total" contains the simulated/measured particle number concentrations ratio from all particle modes, and it is obviously seen that applying model 4 improves the overall global PNSD simulation compared with the sulfuric acid-organic vapor binary model from (Riccobono et al., 2014). This observation shows that including the RH and CS is needed for better understanding of the global particle number size distributions.

6 Conclusion

The particle formation rate is one of the key characteristics in new particle formation studies. By utilizing distinct field measurement data, we can model the particle formation rate and estimate the overall atmospheric aerosol budget over different environments. We parameterized J_5 in four functional forms using the combined datasets from six environments, covering boreal forests (Hyytiälä, Värriö), urban sites (a megacity of Beijing and a large European city of Budapest) and rural environment (Cyprus, Manacapuru). The particle formation schemes involve the main precursor vapor H_2SO_4, relative humidity (RH) and condensation sink (CS). Due to the small number of parameters and the diversity of environments included to generate the schemes, the roles of RH and CS are not only related to their potential direct impact on J_5, but also to sources and sinks of vapors other than H_2SO_4 contributing to formation and growth of sub-5 nm particles and to potential emissions of sub-10 nm particles, e.g., from traffic. Overall, our models showed improved performances as RH and CS were taken into consideration. The model evaluations may suggest that particle formation mechanism is more sensitive to certain factors in specific environments. Sulfuric acid is an effective precursor vapor in NPF processes for most of the measurement sites we selected for model training. Nevertheless, relying solely on H_2SO_4 generally resulted in a weaker model performance for environments where the NPF schemes are dominated by biogenic emissions. This suggests that for developing globally applicable particle formation rate models, more precursor vapor types need to be included alongside H_2SO_4.

The purpose of the paper is twofold: first, to address the lack of knowledge regarding global particle formation rates for particles at 5 nm and larger, and second, to provide a globally applicable semi-empirical parameterization for the sulfuric acid-based neutral particle formation. The simplicity of the parameterization is demonstrated by three factors. First, NPF is a widespread occurrence in various types of environments, where the characteristics of particle formation share common mechanisms involving major precursor types and environmental factors. Second, the main input H_2SO_4 concentrations data can be obtained from field measurements or proxies, from which the

Commented [XL13]: Modification for RC1, Comment 4,5,6 combined. Part 3/6.

contribution of H_2SO_4 to NPF can be directly compared among global sites. Third, we skip the microphysics complexity of sub-5 nm particles, where the physical and chemical properties differ significantly from those that are above 5 nm when discussing particle formation and growth.

The limited data availability from certain sites (less than 1 year), such as Budapest, Cyprus and Manacapuru, should be noted when applying our models. Conclusions drawn from these sites can be more confidently applied to the specific seasons covered in the model training, such as springs being more representable for Budapest and Cyprus, and summer to early autumn for Manacapuru.

Overall, our parameterization findings show that our models including H_2SO_4 concentration, RH and CS can predict J_5 on a satisfactory level for various environment types at once. Among the tested models, models 3 and 4 (Eqs. 4 and 5) can be utilized for predicting J_5 in a global scale if (1) the H_2SO_4 concentrations are known whether through field measurement or proxies, (2) the meteorology parameter RH is monitored continuously, and (3) the particle number size distributions are sufficient and assessed to yield CS. Some caution should be maintained when utilizing these models for environments with very low RH and/or high CS, especially if the high CS is related to primary particle emissions, as the associations between these model parameters and J_5 are complicated and multifaceted. While the parameterizations presented in this study offer an improvement over previous approaches, further development is needed to incorporate vapors important for NPF, such as iodine oxoacids, particularly in marine environments.

Commented [XL14]: Modification for RC1, Comment 4,5,6 combined. Part 6/6.

Commented [XL15]: Modification for RC1, Comment 4,5,6 combined. Part 4/6.

Commented [XL16]: Modification for RC1, Comment 9.

Author contributions. Measurements: NS, RB, CY, LQ, TJ, IS, MV, TW. Data Analysis: XL, LD, MZ, NS, RB, CY, LQ, IS, PZ. Results interpretation: XL, LD, PP, TN. Discussions: all co-authors. Writing: XL, LD, PP, V-MK, TN. Comments and revisions: all co-authors.

Data availability. The datasets used in this study are now available on Zenodo: https://zenodo.org/records/15295592. The data for the 14 global measurement sites are from EBAS database (https://ebas-data.nilu.no/, last access 13.12.2024).

Commented [XL17]: Datasets are now available on Zenodo.

Conflict of interests. At least one of the (co-)authors is a member of the editorial board of Aerosol Research.

Code availability. The MATLAB code used for the parameterization training in this paper is available on Zenodo: https://zenodo.org/records/15295592.

Commented [XL18]: MATLAB code is now available on Zenodo.

Acknowledgements. This work was supported by the European Research Council H2020 projects GASPARCON (Grant No. 714621), FORCeS (Grant No. 821205), and EMME-CARE (Grant No. 856612), by the Cyprus Government, by the Hungarian Research Development and Innovation Office (contract: Advanced 150835), by the Research Council of Finland with grant numbers 355330 and 360114, and by ACCC Flagship funded by the Research Council of Finland grant number 337549. L.D. received funding from the Swiss National Science Foundation (Ambizione grant number 216181). We are grateful to all the people who have contributed to the ambient measurements at measurement stations. The Finnish and Cypriot stations are part of the European research infrastructure ACTRIS. We acknowledge ACTRIS CiGas – Centre for Reactive Trace Gases In Situ Measurements and CAIS-ECAC – Centre for Aerosol In Situ Measurements for providing operational support to the aerosol and reactive trace gas instruments at the stations. We also thank Dr. James N. Smith for providing the GoAmazon2014/5 data for Manacapuru.

Commented [XL19]: Added the missing grand number 821205.

References

Aalto, P., Hämeri, K., Becker, E., Weber, R., Salm, J., Mäkelä, J. M., Hoell, C., O'dowd, C. D., Hansson, H.-C., Väkevä, M., Koponen, I. K., Buzorius, G., and Kulmala, M.: Physical characterization of aerosol particles during nucleation events, Tellus B Chem. Phys. Meteorol., 53, 344–358, https://doi.org/10.3402/tellusb.v53i4.17127, 2001.

Baalbaki, R., Pikridas, M., Jokinen, T., Laurila, T., Dada, L., Bezantakos, S., Ahonen, L., Neitola, K., Maisser, A., Bimenyimana, E., Christodoulou, A., Unga, F., Savvides, C., Lehtipalo, K., Kangasluoma, J., Biskos, G., Petäjä, T., Kerminen, V.-M., Sciare, J., and Kulmala, M.: Towards understanding the characteristics of new particle formation in the Eastern Mediterranean, Atmospheric Chem. Phys., 21, 9223–9251, https://doi.org/10.5194/acp-21-9223-2021, 2021.

Bellouin, N., Quaas, J., Gryspeerdt, E., Kinne, S., Stier, P., Watson-Parris, D., Boucher, O., Carslaw, K. S., Christensen, M., Daniau, A.-L., Dufresne, J.-L., Feingold, G., Fiedler, S., Forster, P., Gettelman, A., Haywood, J. M., Lohmann, U., Malavelle, F., Mauritsen, T., McCoy, D. T., Myhre, G., Mülmenstädt, J., Neubauer, D., Possner, A., Rugenstein, M., Sato, Y., Schulz, M., Schwartz, S. E., Sourdeval, O., Storelvmo, T., Toll, V., Winker, D., and Stevens, B.: Bounding Global Aerosol Radiative Forcing of Climate Change, Rev. Geophys., 58, e2019RG000660, https://doi.org/10.1029/2019RG000660, 2020.

Bergman, T., Makkonen, R., Schrödner, R., Swietlicki, E., Phillips, V. T. J., Le Sager, P., and van Noije, T.: Description and evaluation of a secondary organic aerosol and new particle formation scheme within TM5-MP v1.2, Geosci. Model Dev., 15, 683–713, https://doi.org/10.5194/gmd-15-683-2022, 2022.

Bianchi, F., Kurtén, T., Riva, M., Mohr, C., Rissanen, M. P., Roldin, P., Berndt, T., Crounse, J. D., Wennberg, P. O., Mentel, T. F., Wildt, J., Junninen, H., Jokinen, T., Kulmala, M., Worsnop, D. R., Thornton, J. A., Donahue, N., Kjaergaard, H. G., and

Ehn, M.: Highly Oxygenated Organic Molecules (HOM) from Gas-Phase Autoxidation Involving Peroxy Radicals: A Key Contributor to Atmospheric Aerosol, Chem. Rev., 119, 3472–3509, https://doi.org/10.1021/acs.chemrev.8b00395, 2019.

Bousiotis, D., Pope, F. D., Beddows, D. C. S., Dall'Osto, M., Massling, A., Nøjgaard, J. K., Nordstrøm, C., Niemi, J. V., Portin, H., Petäjä, T., Perez, N., Alastuey, A., Querol, X., Kouvarakis, G., Mihalopoulos, N., Vratolis, S., Eleftheriadis, K., Wiedensohler, A., Weinhold, K., Merkel, M., Tuch, T., and Harrison, R. M.: A phenomenology of new particle formation (NPF) at 13 European sites, Atmospheric Chem. Phys., 21, 11905–11925, https://doi.org/10.5194/acp-21-11905-2021, 2021.

Brean, J., Beddows, D. C. S., Harrison, R. M., Song, C., Tunved, P., Ström, J., Krejci, R., Freud, E., Massling, A., Skov, H., Asmi, E., Lupi, A., and Dall'Osto, M.: Collective geographical ecoregions and precursor sources driving Arctic new particle formation, Atmospheric Chem. Phys., 23, 2183–2198, https://doi.org/10.5194/acp-23-2183-2023, 2023.

Cai, R., Yan, C., Yang, D., Yin, R., Lu, Y., Deng, C., Fu, Y., Ruan, J., Li, X., Kontkanen, J., Zhang, Q., Kangasluoma, J., Ma, Y., Hao, J., Worsnop, D. R., Bianchi, F., Paasonen, P., Kerminen, V.-M., Liu, Y., Wang, L., Zheng, J., Kulmala, M., and Jiang, J.: Sulfuric acid–amine nucleation in urban Beijing, Atmospheric Chem. Phys., 21, 2457–2468, https://doi.org/10.5194/acp-21-2457-2021, 2021.

Cai, R., Deng, C., Stolzenburg, D., Li, C., Guo, J., Kerminen, V.-M., Jiang, J., Kulmala, M., and Kangasluoma, J.: Survival probability of new atmospheric particles: closure between theory and measurements from 1.4 to 100 nm, Atmospheric Chem. Phys., 22, 14571–14587, https://doi.org/10.5194/acp-22-14571-2022, 2022.

Calvo, A. I., Alves, C., Castro, A., Pont, V., Vicente, A. M., and Fraile, R.: Research on aerosol sources and chemical composition: Past, current and emerging issues, Atmospheric Res., 120–121, 1–28, https://doi.org/10.1016/j.atmosres.2012.09.021, 2013.

Chai, T. and Draxler, R. R.: Root mean square error (RMSE) or mean absolute error (MAE)? – Arguments against avoiding RMSE in the literature, Geosci. Model Dev., 7, 1247–1250, https://doi.org/10.5194/gmd-7-1247-2014, 2014.

Chang, L.-S., Schwartz, S. E., McGraw, R., and Lewis, E. R.: Sensitivity of aerosol properties to new particle formation mechanism and to primary emissions in a continental-scale chemical transport model, J. Geophys. Res. Atmospheres, 114, https://doi.org/10.1029/2008JD011019, 2009.

Chen, G., Canonaco, F., Tobler, A., Aas, W., Alastuey, A., Allan, J., Atabakhsh, S., Aurela, M., Baltensperger, U., Bougiatioti, A., De Brito, J. F., Ceburnis, D., Chazeau, B., Chebaicheb, H., Daellenbach, K. R., Ehn, M., El Haddad, I., Eleftheriadis, K., Favez, O., Flentje, H., Font, A., Fossum, K., Freney, E., Gini, M., Green, D. C., Heikkinen, L., Herrmann, H., Kalogridis, A.-C., Keernik, H., Lhotka, R., Lin, C., Lunder, C., Maasikmets, M., Manousakas, M. I., Marchand, N., Marin, C., Marmureanu, L., Mihalopoulos, N., Močnik, G., Nęcki, J., O'Dowd, C., Ovadnevaite, J., Peter, T., Petit, J.-E., Pikridas, M., Matthew Platt, S., Pokorná, P., Poulain, L., Priestman, M., Riffault, V., Rinaldi, M., Różański, K., Schwarz, J., Sciare, J., Simon, L., Skiba, A., Slowik, J. G., Sosedova, Y., Stavroulas, I., Styszko, K., Teinemaa, E., Timonen, H., Tremper, A., Vasilescu, J., Via, M., Vodička, P., Wiedensohler, A., Zografou, O., Cruz Minguillón, M., and Prévôt, A. S. H.: European aerosol phenomenology − 8: Harmonised source apportionment of organic aerosol using 22 Year-long ACSM/AMS datasets, Environ. Int., 166, 107325, https://doi.org/10.1016/j.envint.2022.107325, 2022.

615 Chu, B., Kerminen, V.-M., Bianchi, F., Yan, C., Petäjä, T., and Kulmala, M.: Atmospheric new particle formation in China,
616 Atmospheric Chem. Phys., 19, 115–138, https://doi.org/10.5194/acp-19-115-2019, 2019.
617 Dada, L., Paasonen, P., Nieminen, T., Buenrostro Mazon, S., Kontkanen, J., Peräkylä, O., Lehtipalo, K., Hussein, T., Petäjä,
618 T., Kerminen, V.-M., Bäck, J., and Kulmala, M.: Long-term analysis of clear-sky new particle formation events and nonevents
619 in Hyytiälä, Atmospheric Chem. Phys., 17, 6227–6241, https://doi.org/10.5194/acp-17-6227-2017, 2017.
620 Dada, L., Chellapermal, R., Buenrostro Mazon, S., Paasonen, P., Lampilahti, J., Manninen, H. E., Junninen, H., Petäjä, T.,
621 Kerminen, V.-M., and Kulmala, M.: Refined classification and characterization of atmospheric new-particle formation events
622 using air ions, Atmospheric Chem. Phys., 18, 17883–17893, https://doi.org/10.5194/acp-18-17883-2018, 2018.
623 Dada, L., Ylivinkka, I., Baalbaki, R., Li, C., Guo, Y., Yan, C., Yao, L., Sarnela, N., Jokinen, T., Daellenbach, K. R., Yin, R.,
624 Deng, C., Chu, B., Nieminen, T., Wang, Y., Lin, Z., Thakur, R. C., Kontkanen, J., Stolzenburg, D., Sipilä, M., Hussein, T.,
625 Paasonen, P., Bianchi, F., Salma, I., Weidinger, T., Pikridas, M., Sciare, J., Jiang, J., Liu, Y., Petäjä, T., Kerminen, V.-M., and
626 Kulmala, M.: Sources and sinks driving sulfuric acid concentrations in contrasting environments: implications on proxy
627 calculations, Atmospheric Chem. Phys., 20, 11747–11766, https://doi.org/10.5194/acp-20-11747-2020, 2020.
628 Dal Maso, M., Kulmala, M., Riipinen, I., and Wagner, R.: Formation and growth of fresh atmospheric aerosols: Eight years of
629 aerosol size distribution data from SMEAR II, Hyytiälä, Finland, Boreal Environ. Res., 10, 323–336, 2005.
630 Debevec, C., Sauvage, S., Gros, V., Sellegri, K., Sciare, J., Pikridas, M., Stavroulas, I., Leonardis, T., Gaudion, V., Depelchin,
631 L., Fronval, I., Sarda-Esteve, R., Baisnée, D., Bonsang, B., Savvides, C., Vrekoussis, M., and Locoge, N.: Driving parameters
632 of biogenic volatile organic compounds and consequences on new particle formation observed at an eastern Mediterranean
633 background site, Atmospheric Chem. Phys., 18, 14297–14325, https://doi.org/10.5194/acp-18-14297-2018, 2018.
634 Deng, C., Fu, Y., Dada, L., Yan, C., Cai, R., Yang, D., Zhou, Y., Yin, R., Lu, Y., Li, X., Qiao, X., Fan, X., Nie, W., Kontkanen,
635 J., Kangasluoma, J., Chu, B., Ding, A., Kerminen, V.-M., Paasonen, P., Worsnop, D. R., Bianchi, F., Liu, Y., Zheng, J., Wang,
636 L., Kulmala, M., and Jiang, J.: Seasonal Characteristics of New Particle Formation and Growth in Urban Beijing, Environ.
637 Sci. Technol., 54, 8547–8557, https://doi.org/10.1021/acs.est.0c00808, 2020.
638 Deng, C., Cai, R., Yan, C., Zheng, J., and Jiang, J.: Formation and growth of sub-3 nm particles in megacities: impact of
639 background aerosols, Faraday Discuss., 226, 348–363, https://doi.org/10.1039/D0FD00083C, 2021.
640 Ding, J., Dai, Q., Zhang, Y., Xu, J., Huangfu, Y., and Feng, Y.: Air humidity affects secondary aerosol formation in different
641 pathways, Sci. Total Environ., 759, 143540, https://doi.org/10.1016/j.scitotenv.2020.143540, 2021.
642 Duplissy, J., Merikanto, J., Franchin, A., Tsagkogeorgas, G., Kangasluoma, J., Wimmer, D., Vuollekoski, H., Schobesberger,
643 S., Lehtipalo, K., Flagan, R. C., Brus, D., Donahue, N. M., Vehkamäki, H., Almeida, J., Amorim, A., Barmet, P., Bianchi, F.,
644 Breitenlechner, M., Dunne, E. M., Guida, R., Henschel, H., Junninen, H., Kirkby, J., Kürten, A., Kupc, A., Määttänen, A.,
645 Makhmutov, V., Mathot, S., Nieminen, T., Onnela, A., Praplan, A. P., Riccobono, F., Rondo, L., Steiner, G., Tome, A.,
646 Walther, H., Baltensperger, U., Carslaw, K. S., Dommen, J., Hansel, A., Petäjä, T., Sipilä, M., Stratmann, F., Vrtala, A.,
647 Wagner, P. E., Worsnop, D. R., Curtius, J., and Kulmala, M.: Effect of ions on sulfuric acid-water binary particle formation:

2. Experimental data and comparison with QC-normalized classical nucleation theory, J. Geophys. Res. Atmospheres, 121, 1752–1775, https://doi.org/10.1002/2015JD023539, 2016.

Eisele, F. L. and Tanner, D. J.: Measurement of the gas phase concentration of H2SO4 and methane sulfonic acid and estimates of H2SO4 production and loss in the atmosphere, J. Geophys. Res. Atmospheres, 98, 9001–9010, https://doi.org/10.1029/93JD00031, 1993.

Glasoe, W. A., Volz, K., Panta, B., Freshour, N., Bachman, R., Hanson, D. R., McMurry, P. H., and Jen, C.: Sulfuric acid nucleation: An experimental study of the effect of seven bases, J. Geophys. Res. Atmospheres, 120, 1933–1950, https://doi.org/10.1002/2014JD022730, 2015.

Gordon, H., Kirkby, J., Baltensperger, U., Bianchi, F., Breitenlechner, M., Curtius, J., Dias, A., Dommen, J., Donahue, N. M., Dunne, E. M., Duplissy, J., Ehrhart, S., Flagan, R. C., Frege, C., Fuchs, C., Hansel, A., Hoyle, C. R., Kulmala, M., Kürten, A., Lehtipalo, K., Makhmutov, V., Molteni, U., Rissanen, M. P., Stozkhov, Y., Tröstl, J., Tsagkogeorgas, G., Wagner, R., Williamson, C., Wimmer, D., Winkler, P. M., Yan, C., and Carslaw, K. S.: Causes and importance of new particle formation in the present-day and preindustrial atmospheres, J. Geophys. Res. Atmospheres, 122, 8739–8760, https://doi.org/10.1002/2017JD026844, 2017.

Hamed, A., Korhonen, H., Sihto, S.-L., Joutsensaari, J., Järvinen, H., Petäjä, T., Arnold, F., Nieminen, T., Kulmala, M., Smith, J. N., Lehtinen, K. E. J., and Laaksonen, A.: The role of relative humidity in continental new particle formation, J. Geophys. Res. Atmospheres, 116, https://doi.org/10.1029/2010JD014186, 2011.

Hari, P. and Kulmala, M.: Station for measuring Ecosystem-Atmosphere relations (SMEAR II), Boreal Environ. Res., 10, 2005.

He, X.-C., Tham, Y. J., Dada, L., Wang, M., Finkenzeller, H., Stolzenburg, D., Iyer, S., Simon, M., Kürten, A., Shen, J., Rörup, B., Rissanen, M., Schobesberger, S., Baalbaki, R., Wang, D. S., Koenig, T. K., Jokinen, T., Sarnela, N., Beck, L. J., Almeida, J., Amanatidis, S., Amorim, A., Ataei, F., Baccarini, A., Bertozzi, B., Bianchi, F., Brilke, S., Caudillo, L., Chen, D., Chiu, R., Chu, B., Dias, A., Ding, A., Dommen, J., Duplissy, J., El Haddad, I., Gonzalez Carracedo, L., Granzin, M., Hansel, A., Heinritzi, M., Hofbauer, V., Junninen, H., Kangasluoma, J., Kemppainen, D., Kim, C., Kong, W., Krechmer, J. E., Kvashin, A., Laitinen, T., Lamkaddam, H., Lee, C. P., Lehtipalo, K., Leiminger, M., Li, Z., Makhmutov, V., Manninen, H. E., Marie, G., Marten, R., Mathot, S., Mauldin, R. L., Mentler, B., Möhler, O., Müller, T., Nie, W., Onnela, A., Petäjä, T., Pfeifer, J., Philippov, M., Ranjithkumar, A., Saiz-Lopez, A., Salma, I., Scholz, W., Schuchmann, S., Schulze, B., Steiner, G., Stozhkov, Y., Tauber, C., Tomé, A., Thakur, R. C., Väisänen, O., Vazquez-Pufleau, M., Wagner, A. C., Wang, Y., Weber, S. K., Winkler, P. M., Wu, Y., Xiao, M., Yan, C., Ye, Q., Ylisirniö, A., Zauner-Wieczorek, M., Zha, Q., Zhou, P., Flagan, R. C., Curtius, J., Baltensperger, U., Kulmala, M., Kerminen, V.-M., Kurtén, T., et al.: Role of iodine oxoacids in atmospheric aerosol nucleation, Science, 371, 589–595, https://doi.org/10.1126/science.abe0298, 2021.

Heinritzi, M., Dada, L., Simon, M., Stolzenburg, D., Wagner, A. C., Fischer, L., Ahonen, L. R., Amanatidis, S., Baalbaki, R., Baccarini, A., Bauer, P. S., Baumgartner, B., Bianchi, F., Brilke, S., Chen, D., Chiu, R., Dias, A., Dommen, J., Duplissy, J., Finkenzeller, H., Frege, C., Fuchs, C., Garmash, O., Gordon, H., Granzin, M., El Haddad, I., He, X., Helm, J., Hofbauer, V.,

682 Hoyle, C. R., Kangasluoma, J., Keber, T., Kim, C., Kürten, A., Lamkaddam, H., Laurila, T. M., Lampilahti, J., Lee, C. P.,
683 Lehtipalo, K., Leiminger, M., Mai, H., Makhmutov, V., Manninen, H. E., Marten, R., Mathot, S., Mauldin, R. L., Mentler, B.,
684 Molteni, U., Müller, T., Nie, W., Nieminen, T., Onnela, A., Partoll, E., Passananti, M., Petäjä, T., Pfeifer, J., Pospisilova, V.,
685 Quéléver, L. L. J., Rissanen, M. P., Rose, C., Schobesberger, S., Scholz, W., Scholze, K., Sipilä, M., Steiner, G., Stozhkov,
686 Y., Tauber, C., Tham, Y. J., Vazquez-Pufleau, M., Virtanen, A., Vogel, A. L., Volkamer, R., Wagner, R., Wang, M., Weitz,
687 L., Wimmer, D., Xiao, M., Yan, C., Ye, P., Zha, Q., Zhou, X., Amorim, A., Baltensperger, U., Hansel, A., Kulmala, M., Tomé,
688 A., Winkler, P. M., Worsnop, D. R., Donahue, N. M., Kirkby, J., and Curtius, J.: Molecular understanding of the suppression
689 of new-particle formation by isoprene, Atmospheric Chem. Phys., 20, 11809–11821, https://doi.org/10.5194/acp-20-11809-
690 2020, 2020.
691 Hellmuth, O.: Columnar modelling of nucleation burst evolution in the convective boundary layer – first results from a
692 feasibility study Part I: Modelling approach, Atmospheric Chem. Phys., 6, 4175–4214, https://doi.org/10.5194/acp-6-4175-
693 2006, 2006.
694 Huijnen, V., Williams, J., van Weele, M., van Noije, T., Krol, M., Dentener, F., Segers, A., Houweling, S., Peters, W., de Laat,
695 J., Boersma, F., Bergamaschi, P., van Velthoven, P., Le Sager, P., Eskes, H., Alkemade, F., Scheele, R., Nédélec, P., and Pätz,
696 H.-W.: The global chemistry transport model TM5: description and evaluation of the tropospheric chemistry version 3.0,
697 Geosci. Model Dev., 3, 445–473, https://doi.org/10.5194/gmd-3-445-2010, 2010.
698 Jiang, B. and Xia, D.: Role identification of NH3 in atmospheric secondary new particle formation in haze occurrence of
699 China, Atmos. Environ., 163, 107–117, https://doi.org/10.1016/j.atmosenv.2017.05.035, 2017.
700 Jokinen, T., Sipilä, M., Junninen, H., Ehn, M., Lönn, G., Hakala, J., Petäjä, T., Mauldin, R. L. I., Kulmala, M., and Worsnop,
701 D. R.: Atmospheric sulphuric acid and neutral cluster measurements using CI-APi-TOF, Atmospheric Chem. Phys., 12, 4117–
702 4125, https://doi.org/10.5194/acp-12-4117-2012, 2012.
703 Jokinen, T., Lehtipalo, K., Thakur, R. C., Ylivinkka, I., Neitola, K., Sarnela, N., Laitinen, T., Kulmala, M., Petäjä, T., and
704 Sipilä, M.: Measurement report: Long-term measurements of aerosol precursor concentrations in the Finnish subarctic boreal
705 forest, Atmospheric Chem. Phys., 22, 2237–2254, https://doi.org/10.5194/acp-22-2237-2022, 2022.
706 Junninen, H., Ehn, M., Petäjä, T., Luosujärvi, L., Kotiaho, T., Kostiainen, R., Rohner, U., Gonin, M., Fuhrer, K., Kulmala, M.,
707 and Worsnop, D. R.: A high-resolution mass spectrometer to measure atmospheric ion composition, Atmospheric Meas. Tech.,
708 3, 1039–1053, https://doi.org/10.5194/amt-3-1039-2010, 2010.
709 Kerminen, V.-M. and Kulmala, M.: Analytical formulae connecting the “real” and the “apparent” nucleation rate and the nuclei
710 number concentration for atmospheric nucleation events, J. Aerosol Sci., 33, 609–622, https://doi.org/10.1016/S0021-
711 8502(01)00194-X, 2002.
712 Kerminen, V.-M., Chen, X., Vakkari, V., Petäjä, T., Kulmala, M., and Bianchi, F.: Atmospheric new particle formation and
713 growth: review of field observations, Environ. Res. Lett., 13, 103003, https://doi.org/10.1088/1748-9326/aadf3c, 2018.

714 Kiendler-Scharr, A., Wildt, J., Maso, M. D., Hohaus, T., Kleist, E., Mentel, T. F., Tillmann, R., Uerlings, R., Schurr, U., and
715 Wahner, A.: New particle formation in forests inhibited by isoprene emissions, Nature, 461, 381–384,
716 https://doi.org/10.1038/nature08292, 2009.
717 Kirkby, J., Curtius, J., Almeida, J., Dunne, E., Duplissy, J., Ehrhart, S., Franchin, A., Gagné, S., Ickes, L., Kürten, A., Kupc,
718 A., Metzger, A., Riccobono, F., Rondo, L., Schobesberger, S., Tsagkogeorgas, G., Wimmer, D., Amorim, A., Bianchi, F.,
719 Breitenlechner, M., David, A., Dommen, J., Downard, A., Ehn, M., Flagan, R. C., Haider, S., Hansel, A., Hauser, D., Jud, W.,
720 Junninen, H., Kreissl, F., Kvashin, A., Laaksonen, A., Lehtipalo, K., Lima, J., Lovejoy, E. R., Makhmutov, V., Mathot, S.,
721 Mikkilä, J., Minginette, P., Mogo, S., Nieminen, T., Onnela, A., Pereira, P., Petäjä, T., Schnitzhofer, R., Seinfeld, J. H., Sipilä,
722 M., Stozhkov, Y., Stratmann, F., Tomé, A., Vanhanen, J., Viisanen, Y., Vrtala, A., Wagner, P. E., Walther, H., Weingartner,
723 E., Wex, H., Winkler, P. M., Carslaw, K. S., Worsnop, D. R., Baltensperger, U., and Kulmala, M.: Role of sulphuric acid,
724 ammonia and galactic cosmic rays in atmospheric aerosol nucleation, Nature, 476, 429–433,
725 https://doi.org/10.1038/nature10343, 2011.
726 Kleindienst, T. E.: Epoxying Isoprene Chemistry, Science, 325, 687–688, https://doi.org/10.1126/science.1178324, 2009.
727 Kulmala, M., Maso, M. D., Mäkelä, J. M., Pirjola, L., Väkevä, M., Aalto, P., Miikkulainen, P., Hämeri, K., and O'dowd, C.
728 D.: On the formation, growth and composition of nucleation mode particles, Tellus B, 53, 479–490,
729 https://doi.org/10.1034/j.1600-0889.2001.530411.x, 2001.
730 Kulmala, M., Vehkamäki, H., Petäjä, T., Dal Maso, M., Lauri, A., Kerminen, V.-M., Birmili, W., and McMurry, P. H.:
731 Formation and growth rates of ultrafine atmospheric particles: a review of observations, J. Aerosol Sci., 35, 143–176,
732 https://doi.org/10.1016/j.jaerosci.2003.10.003, 2004.
733 Kulmala, M., Lehtinen, K. E. J., and Laaksonen, A.: Cluster activation theory as an explanation of the linear dependence
734 between formation rate of 3nm particles and sulphuric acid concentration, Atmospheric Chem. Phys., 6, 787–793,
735 https://doi.org/10.5194/acp-6-787-2006, 2006.
736 Kulmala, M., Petäjä, T., Nieminen, T., Sipilä, M., Manninen, H. E., Lehtipalo, K., Dal Maso, M., Aalto, P. P., Junninen, H.,
737 Paasonen, P., Riipinen, I., Lehtinen, K. E. J., Laaksonen, A., and Kerminen, V.-M.: Measurement of the nucleation of
738 atmospheric aerosol particles, Nat. Protoc., 7, 1651–1667, https://doi.org/10.1038/nprot.2012.091, 2012.
739 Kulmala, M., Kontkanen, J., Junninen, H., Lehtipalo, K., Manninen, H. E., Nieminen, T., Petäjä, T., Sipilä, M., Schobesberger,
740 S., Rantala, P., Franchin, A., Jokinen, T., Järvinen, E., Äijälä, M., Kangasluoma, J., Hakala, J., Aalto, P. P., Paasonen, P.,
741 Mikkilä, J., Vanhanen, J., Aalto, J., Hakola, H., Makkonen, U., Ruuskanen, T., Mauldin, R. L., Duplissy, J., Vehkamäki, H.,
742 Bäck, J., Kortelainen, A., Riipinen, I., Kurtén, T., Johnston, M. V., Smith, J. N., Ehn, M., Mentel, T. F., Lehtinen, K. E. J.,
743 Laaksonen, A., Kerminen, V.-M., and Worsnop, D. R.: Direct Observations of Atmospheric Aerosol Nucleation, Science, 339,
744 943–946, https://doi.org/10.1126/science.1227385, 2013.
745 Kulmala, M., Kerminen, V.-M., Petäjä, T., J. Ding, A., and Wang, L.: Atmospheric gas-to-particle conversion: why NPF events
746 are observed in megacities?, Faraday Discuss., 200, 271–288, https://doi.org/10.1039/C6FD00257A, 2017.

Kulmala, M., Junninen, H., Dada, L., Salma, I., Weidinger, T., Thén, W., Vörösmarty, M., Komsaare, K., Stolzenburg, D., Cai, R., Yan, C., Li, X., Deng, C., Jiang, J., Petäjä, T., Nieminen, T., and Kerminen, V.-M.: Quiet New Particle Formation in the Atmosphere, Front. Environ. Sci., 10, 2022a.

Kulmala, M., Cai, R., Stolzenburg, D., Zhou, Y., Dada, L., Guo, Y., Yan, C., Petäjä, T., Jiang, J., and Kerminen, V.-M.: The contribution of new particle formation and subsequent growth to haze formation, Environ. Sci. Atmospheres, 2, 352–361, https://doi.org/10.1039/D1EA00096A, 2022b.

Kulmala, M., Cai, R., Ezhova, E., Deng, C., Stolzenburg, D., Dada, L., Guo, Y., Chao, Y., Peräkylä, O., Lintunen, A., Nieminen, T., Kokkonen, T. V., Sarnela, N., and Kerminen, T. P. & V.-M.: Direct link between the characteristics of atmospheric new particle formation and Continental Biosphere-Atmosphere-Cloud-Climate (COBACC) feedback loop, Boreal Environ. Res., 28, 1–13, 2023.

Kürten, A., Rondo, L., Ehrhart, S., and Curtius, J.: Calibration of a Chemical Ionization Mass Spectrometer for the Measurement of Gaseous Sulfuric Acid, J. Phys. Chem. A, 116, 6375–6386, https://doi.org/10.1021/jp212123n, 2012.

Kyrö, E.-M., Väänänen, R., Kerminen, V.-M., Virkkula, A., Petäjä, T., Asmi, A., Dal Maso, M., Nieminen, T., Juhola, S., Shcherbinin, A., Riipinen, I., Lehtipalo, K., Keronen, P., Aalto, P. P., Hari, P., and Kulmala, M.: Trends in new particle formation in eastern Lapland, Finland: effect of decreasing sulfur emissions from Kola Peninsula, Atmospheric Chem. Phys., 14, 4383–4396, https://doi.org/10.5194/acp-14-4383-2014, 2014.

Laakso, L., Petaja, T., Lehtinen, K. E. J., Kulmala, M., Paatero, J., Horrak, U., Tammet, H., and Joutsensaari, J.: Ion production rate in a boreal forest based on ion, particle and radiation measurements, Atmos Chem Phys, 11, 2004.

Laarne, P., Amnell, E., Zaidan, M. A., Mikkonen, S., and Nieminen, T.: Exploring Non-Linear Dependencies in Atmospheric Data with Mutual Information, Atmosphere, 13, 1046, https://doi.org/10.3390/atmos13071046, 2022.

Lan, Z., Lin, W., Pu, W., and Ma, Z.: Measurement report: Exploring NH₃ behavior in urban and suburban Beijing: comparison and implications, Atmospheric Chem. Phys., 21, 4561–4573, https://doi.org/10.5194/acp-21-4561-2021, 2021.

Lee, S.-H., Gordon, H., Yu, H., Lehtipalo, K., Haley, R., Li, Y., and Zhang, R.: New Particle Formation in the Atmosphere: From Molecular Clusters to Global Climate, J. Geophys. Res. Atmospheres, 124, 7098–7146, https://doi.org/10.1029/2018JD029356, 2019.

Lehtinen, K. E. J. and Kulmala, M.: A model for particle formation and growth in the atmosphere with molecular resolution in size, Atmos Chem Phys, 7, 2003.

Lehtipalo, K., Yan, C., Dada, L., Bianchi, F., Xiao, M., Wagner, R., Stolzenburg, D., Ahonen, L. R., Amorim, A., Baccarini, A., Bauer, P. S., Baumgartner, B., Bergen, A., Bernhammer, A.-K., Breitenlechner, M., Brilke, S., Buchholz, A., Mazon, S. B., Chen, D., Chen, X., Dias, A., Dommen, J., Draper, D. C., Duplissy, J., Ehn, M., Finkenzeller, H., Fischer, L., Frege, C., Fuchs, C., Garmash, O., Gordon, H., Hakala, J., He, X., Heikkinen, L., Heinritzi, M., Helm, J. C., Hofbauer, V., Hoyle, C. R., Jokinen, T., Kangasluoma, J., Kerminen, V.-M., Kim, C., Kirkby, J., Kontkanen, J., Kürten, A., Lawler, M. J., Mai, H., Mathot, S., Mauldin, R. L., Molteni, U., Nichman, L., Nie, W., Nieminen, T., Ojdanic, A., Onnela, A., Passananti, M., Petäjä, T., Piel,

F., Pospisilova, V., Quéléver, L. L. J., Rissanen, M. P., Rose, C., Sarnela, N., Schallhart, S., Schuchmann, S., Sengupta, K., Simon, M., Sipilä, M., Tauber, C., Tomé, A., Tröstl, J., Väisänen, O., Vogel, A. L., Volkamer, R., Wagner, A. C., Wang, M., Weitz, L., Wimmer, D., Ye, P., Ylisirniö, A., Zha, Q., Carslaw, K. S., Curtius, J., Donahue, N. M., Flagan, R. C., Hansel, A., Riipinen, I., Virtanen, A., Winkler, P. M., Baltensperger, U., Kulmala, M., and Worsnop, D. R.: Multicomponent new particle formation from sulfuric acid, ammonia, and biogenic vapors, Sci. Adv., 4, eaau5363, https://doi.org/10.1126/sciadv.aau5363, 2018.

Li, X., Chee, S., Hao, J., Abbatt, J. P. D., Jiang, J., and Smith, J. N.: Relative humidity effect on the formation of highly oxidized molecules and new particles during monoterpene oxidation, Atmospheric Chem. Phys., 19, 1555–1570, https://doi.org/10.5194/acp-19-1555-2019, 2019.

Liu, Q., Jia, X., Quan, J., Li, J., Li, X., Wu, Y., Chen, D., Wang, Z., and Liu, Y.: New positive feedback mechanism between boundary layer meteorology and secondary aerosol formation during severe haze events, Sci. Rep., 8, 6095, https://doi.org/10.1038/s41598-018-24366-3, 2018.

Liu, Y., Yan, C., Feng, Z., Zheng, F., Fan, X., Zhang, Y., Li, C., Zhou, Y., Lin, Z., Guo, Y., Zhang, Y., Ma, L., Zhou, W., Liu, Z., Dada, L., Dällenbach, K., Kontkanen, J., Cai, R., Chan, T., Chu, B., Du, W., Yao, L., Wang, Y., Cai, J., Kangasluoma, J., Kokkonen, T., Kujansuu, J., Rusanen, A., Deng, C., Fu, Y., Yin, R., Li, X., Lu, Y., Liu, Y., Lian, C., Yang, D., Wang, W., Ge, M., Wang, Y., Worsnop, D. R., Junninen, H., He, H., Kerminen, V.-M., Zheng, J., Wang, L., Jiang, J., Petäjä, T., Bianchi, F., and Kulmala, M.: Continuous and comprehensive atmospheric observations in Beijing: a station to understand the complex urban atmospheric environment, Big Earth Data, 4, 295–321, https://doi.org/10.1080/20964471.2020.1798707, 2020.

Määttänen, A., Merikanto, J., Henschel, H., Duplissy, J., Makkonen, R., Ortega, I. K., and Vehkamäki, H.: New Parameterizations for Neutral and Ion-Induced Sulfuric Acid-Water Particle Formation in Nucleation and Kinetic Regimes, J. Geophys. Res. Atmospheres, 123, 1269–1296, https://doi.org/10.1002/2017JD027429, 2018.

Marten, R., Xiao, M., Rörup, B., Wang, M., Kong, W., He, X.-C., Stolzenburg, D., Pfeifer, J., Marie, G., S. Wang, D., Scholz, W., Baccarini, A., Ping Lee, C., Amorim, A., Baalbaki, R., M. Bell, D., Bertozzi, B., Caudillo, L., Chu, B., Dada, L., Duplissy, J., Finkenzeller, H., Gonzalez Carracedo, L., Granzin, M., Hansel, A., Heinritzi, M., Hofbauer, V., Kemppainen, D., Kürten, A., Lampimäki, M., Lehtipalo, K., Makhmutov, V., E. Manninen, H., Mentler, B., Petäjä, T., Philippov, M., Shen, J., Simon, M., Stozhkov, Y., Tomé, A., C. Wagner, A., Wang, Y., K. Weber, S., Wu, Y., Zauner-Wieczorek, M., Curtius, J., Kulmala, M., Möhler, O., Volkamer, R., M. Winkler, P., R. Worsnop, D., Dommen, J., C. Flagan, R., Kirkby, J., M. Donahue, N., Lamkaddam, H., Baltensperger, U., and Haddad, I. E.: Survival of newly formed particles in haze conditions, Environ. Sci. Atmospheres, 2, 491–499, https://doi.org/10.1039/D2EA00007E, 2022.

Martin, S. T., Artaxo, P., Machado, L. a. T., Manzi, A. O., Souza, R. a. F., Schumacher, C., Wang, J., Andreae, M. O., Barbosa, H. M. J., Fan, J., Fisch, G., Goldstein, A. H., Guenther, A., Jimenez, J. L., Pöschl, U., Silva Dias, M. A., Smith, J. N., and Wendisch, M.: Introduction: Observations and Modeling of the Green Ocean Amazon (GoAmazon2014/5), Atmospheric Chem. Phys., 16, 4785–4797, https://doi.org/10.5194/acp-16-4785-2016, 2016.

Mauldin III, R. L., Frost, G. J., Chen, G., Tanner, D. J., Prevot, A. S. H., Davis, D. D., and Eisele, F. L.: OH measurements during the First Aerosol Characterization Experiment (ACE 1): Observations and model comparisons, J. Geophys. Res. Atmospheres, 103, 16713–16729, https://doi.org/10.1029/98JD00882, 1998.

Mazon, S. B., Kontkanen, J., Manninen, H. E., Nieminen, T., Kerminen, V.-M., and Kulmala, M.: A long-term comparison of nighttime cluster events and daytime ion formation in a boreal forest, 2016.

McMurry, P. H. and Friedlander, S. K.: New particle formation in the presence of an aerosol, Atmospheric Environ. 1967, 13, 1635–1651, https://doi.org/10.1016/0004-6981(79)90322-6, 1979.

Myers, D. C., Kim, S., Sjostedt, S., Guenther, A. B., Seco, R., Vega Bustillos, O., Tota, J., Souza, R. A. F., and Smith, J. N.: Sulfuric acid in the Amazon basin: measurements and evaluation of existing sulfuric acid proxies, Atmospheric Chem. Phys., 22, 10061–10076, https://doi.org/10.5194/acp-22-10061-2022, 2022.

Myllys, N., Kubečka, J., Besel, V., Alfaouri, D., Olenius, T., Smith, J. N., and Passananti, M.: Role of base strength, cluster structure and charge in sulfuric-acid-driven particle formation, Atmospheric Chem. Phys., 19, 9753–9768, https://doi.org/10.5194/acp-19-9753-2019, 2019.

Neefjes, I., Laapas, M., Liu, Y., Medus, E., Miettunen, E., Ahonen, L., Quelever, L., Aalto, J., Bäck, J., Kerminen, V.-M., Lampilahti, J., Luoma, K., Mäki, M., Mammarella, I., Petäjä, T., Räty, M., Sarnela, N., Ylivinkka, I., Hakala, S., Kulmala, M., Nieminen, T., and Lintunen, A.: 25 years of atmospheric and ecosystem measurements in a boreal forest - Seasonal variation and responses to warm and dry years, Boreal Environ. Res., 27, 1–31, 2022.

Nieminen, T., Paasonen, P., Manninen, H. E., Sellegri, K., Kerminen, V.-M., and Kulmala, M.: Parameterization of ion-induced nucleation rates based on ambient observations, Atmospheric Chem. Phys., 11, 3393–3402, https://doi.org/10.5194/acp-11-3393-2011, 2011.

Nieminen, T., Yli-Juuti, T., Manninen, H. E., Petäjä, T., Kerminen, V.-M., and Kulmala, M.: Technical note: New particle formation event forecasts during PEGASOS–Zeppelin Northern mission 2013 in Hyytiälä, Finland, Atmospheric Chem. Phys., 15, 12385–12396, https://doi.org/10.5194/acp-15-12385-2015, 2015.

Nieminen, T., Kerminen, V.-M., Petäjä, T., Aalto, P. P., Arshinov, M., Asmi, E., Baltensperger, U., Beddows, D. C. S., Beukes, J. P., Collins, D., Ding, A., Harrison, R. M., Henzing, B., Hooda, R., Hu, M., Hõrrak, U., Kivekäs, N., Komsaare, K., Krejci, R., Kristensson, A., Laakso, L., Laaksonen, A., Leaitch, W. R., Lihavainen, H., Mihalopoulos, N., Németh, Z., Nie, W., O'Dowd, C., Salma, I., Sellegri, K., Svenningsson, B., Swietlicki, E., Tunved, P., Ulevicius, V., Vakkari, V., Vana, M., Wiedensohler, A., Wu, Z., Virtanen, A., and Kulmala, M.: Global analysis of continental boundary layer new particle formation based on long-term measurements, Atmospheric Chem. Phys., 18, 14737–14756, https://doi.org/10.5194/acp-18-14737-2018, 2018.

Okuljar, M., Kuuluvainen, H., Kontkanen, J., Garmash, O., Olin, M., Niemi, J. V., Timonen, H., Kangasluoma, J., Tham, Y. J., Baalbaki, R., Sipilä, M., Salo, L., Lintusaari, H., Portin, H., Teinilä, K., Aurela, M., Dal Maso, M., Rönkkö, T., Petäjä, T., and Paasonen, P.: Measurement report: The influence of traffic and new particle formation on the size distribution of 1–

800 nm particles in Helsinki – a street canyon and an urban background station comparison, Atmospheric Chem. Phys., 21, 9931–9953, https://doi.org/10.5194/acp-21-9931-2021, 2021.

Paasonen, P., Nieminen, T., Asmi, E., Manninen, H. E., Petäjä, T., Plass-Dülmer, C., Flentje, H., Birmili, W., Wiedensohler, A., Hörrak, U., Metzger, A., Hamed, A., Laaksonen, A., Facchini, M. C., Kerminen, V.-M., and Kulmala, M.: On the roles of sulphuric acid and low-volatility organic vapours in the initial steps of atmospheric new particle formation, Atmospheric Chem. Phys., 10, 11223–11242, https://doi.org/10.5194/acp-10-11223-2010, 2010.

Paulot, F., Crounse, J. D., Kjaergaard, H. G., Kürten, A., St. Clair, J. M., Seinfeld, J. H., and Wennberg, P. O.: Unexpected Epoxide Formation in the Gas-Phase Photooxidation of Isoprene, Science, 325, 730–733, https://doi.org/10.1126/science.1172910, 2009.

Petters, M. D. and Kreidenweis, S. M.: A single parameter representation of hygroscopic growth and cloud condensation nucleus activity, Atmospheric Chem. Phys., 7, 1961–1971, https://doi.org/10.5194/acp-7-1961-2007, 2007.

Quéléver, L. L. J., Dada, L., Asmi, E., Lampilahti, J., Chan, T., Ferrara, J. E., Copes, G. E., Pérez-Fogwill, G., Barreira, L., Aurela, M., Worsnop, D. R., Jokinen, T., and Sipilä, M.: Investigation of new particle formation mechanisms and aerosol processes at Marambio Station, Antarctic Peninsula, Atmospheric Chem. Phys., 22, 8417–8437, https://doi.org/10.5194/acp-22-8417-2022, 2022.

Riccobono, F., Schobesberger, S., Scott, C. E., Dommen, J., Ortega, I. K., Rondo, L., Almeida, J., Amorim, A., Bianchi, F., Breitenlechner, M., David, A., Downard, A., Dunne, E. M., Duplissy, J., Ehrhart, S., Flagan, R. C., Franchin, A., Hansel, A., Junninen, H., Kajos, M., Keskinen, H., Kupc, A., Kürten, A., Kvashin, A. N., Laaksonen, A., Lehtipalo, K., Makhmutov, V., Mathot, S., Nieminen, T., Onnela, A., Petäjä, T., Praplan, A. P., Santos, F. D., Schallhart, S., Seinfeld, J. H., Sipilä, M., Spracklen, D. V., Stozhkov, Y., Stratmann, F., Tomé, A., Tsagkogeorgas, G., Vaattovaara, P., Viisanen, Y., Vrtala, A., Wagner, P. E., Weingartner, E., Wex, H., Wimmer, D., Carslaw, K. S., Curtius, J., Donahue, N. M., Kirkby, J., Kulmala, M., Worsnop, D. R., and Baltensperger, U.: Oxidation Products of Biogenic Emissions Contribute to Nucleation of Atmospheric Particles, Science, 344, 717–721, https://doi.org/10.1126/science.1243527, 2014.

Roldin, P., Swietlicki, E., Massling, A., Kristensson, A., Löndahl, J., Eriksson, A., Pagels, J., and Gustafsson, S.: Aerosol ageing in an urban plume – implication for climate, Atmospheric Chem. Phys., 11, 5897–5915, https://doi.org/10.5194/acp-11-5897-2011, 2011.

Rönkkö, T., Kuuluvainen, H., Karjalainen, P., Keskinen, J., Hillamo, R., Niemi, J. V., Pirjola, L., Timonen, H. J., Saarikoski, S., Saukko, E., Järvinen, A., Silvennoinen, H., Rostedt, A., Olin, M., Yli-Ojanperä, J., Nousiainen, P., Kousa, A., and Dal Maso, M.: Traffic is a major source of atmospheric nanocluster aerosol, Proc. Natl. Acad. Sci., 114, 7549–7554, https://doi.org/10.1073/pnas.1700830114, 2017.

Rosati, B., Christiansen, S., Wollesen de Jonge, R., Roldin, P., Jensen, M. M., Wang, K., Moosakutty, S. P., Thomsen, D., Salomonsen, C., Hyttinen, N., Elm, J., Feilberg, A., Glasius, M., and Bilde, M.: New Particle Formation and Growth from Dimethyl Sulfide Oxidation by Hydroxyl Radicals, ACS Earth Space Chem., 5, 801–811, https://doi.org/10.1021/acsearthspacechem.0c00333, 2021.

881 Ruosteenoja, K. and Räisänen, P.: Seasonal Changes in Solar Radiation and Relative Humidity in Europe in Response to
882 Global Warming, J. Clim., 26, 2467–2481, https://doi.org/10.1175/JCLI-D-12-00007.1, 2013.
883 Salma, I. and Németh, Z.: Dynamic and timing properties of new aerosol particle formation and consecutive growth events,
884 Atmospheric Chem. Phys., 19, 5835–5852, https://doi.org/10.5194/acp-19-5835-2019, 2019.
885 Salma, I., Borsós, T., Weidinger, T., Aalto, P., Hussein, T., Dal Maso, M., and Kulmala, M.: Production, growth and properties
886 of ultrafine atmospheric aerosol particles in an urban environment, Atmospheric Chem. Phys., 11, 1339–1353,
887 https://doi.org/10.5194/acp-11-1339-2011, 2011.
888 Salma, I., Németh, Z., Kerminen, V.-M., Aalto, P., Nieminen, T., Weidinger, T., Molnár, Á., Imre, K., and Kulmala, M.:
889 Regional effect on urban atmospheric nucleation, Atmospheric Chem. Phys., 16, 8715–8728, https://doi.org/10.5194/acp-16-
890 8715-2016, 2016.
891 Salma, I., Thén, W., Aalto, P., Kerminen, V.-M., Kern, A., Barcza, Z., Petäjä, T., and Kulmala, M.: Influence of vegetation on
892 occurrence and time distributions of regional new aerosol particle formation and growth, Atmospheric Chem. Phys., 21, 2861–
893 2880, https://doi.org/10.5194/acp-21-2861-2021, 2021.
894 Sanchez, K. J., Russell, L. M., Modini, R. L., Frossard, A. A., Ahlm, L., Corrigan, C. E., Roberts, G. C., Hawkins, L. N.,
895 Schroder, J. C., Bertram, A. K., Zhao, R., Lee, A. K. Y., Lin, J. J., Nenes, A., Wang, Z., Wonaschütz, A., Sorooshian, A.,
896 Noone, K. J., Jonsson, H., Toom, D., Macdonald, A. M., Leaitch, W. R., and Seinfeld, J. H.: Meteorological and aerosol effects
897 on marine cloud microphysical properties, J. Geophys. Res. Atmospheres, 121, 4142–4161,
898 https://doi.org/10.1002/2015JD024595, 2016.
899 Schiro, K. A., Ahmed, F., Giangrande, S. E., and Neelin, J. D.: GoAmazon2014/5 campaign points to deep-inflow approach
900 to deep convection across scales, Proc. Natl. Acad. Sci., 115, 4577–4582, https://doi.org/10.1073/pnas.1719842115, 2018.
901 Sihto, S.-L., Kulmala, M., Kerminen, V.-M., Dal Maso, M., Petäjä, T., Riipinen, I., Korhonen, H., Arnold, F., Janson, R., Boy,
902 M., Laaksonen, A., and Lehtinen, K. E. J.: Atmospheric sulphuric acid and aerosol formation: implications from atmospheric
903 measurements for nucleation and early growth mechanisms, Atmospheric Chem. Phys., 6, 4079–4091,
904 https://doi.org/10.5194/acp-6-4079-2006, 2006.
905 Spracklen, D. V., Bonn, B., and Carslaw, K. S.: Boreal forests, aerosols and the impacts on clouds and climate, Philos. Trans.
906 R. Soc. Math. Phys. Eng. Sci., 366, 4613–4626, https://doi.org/10.1098/rsta.2008.0201, 2008.
907 Tunved, P., Hansson, H.-C., Kerminen, V.-M., Ström, J., Maso, M. D., Lihavainen, H., Viisanen, Y., Aalto, P. P., Komppula,
908 M., and Kulmala, M.: High Natural Aerosol Loading over Boreal Forests, Science, 312, 261–263,
909 https://doi.org/10.1126/science.1123052, 2006.
910 Tuovinen, S., Kontkanen, J., Jiang, J., and Kulmala, M.: Investigating the effectiveness of condensation sink based on
911 heterogeneous nucleation theory, J. Aerosol Sci., 149, 105613, https://doi.org/10.1016/j.jaerosci.2020.105613, 2020.
912 Tuovinen, S., Cai, R., Kerminen, V.-M., Jiang, J., Yan, C., Kulmala, M., and Kontkanen, J.: Survival probabilities of
913 atmospheric particles: comparison based on theory, cluster population simulations, and observations in Beijing, Atmospheric
914 Chem. Phys., 22, 15071–15091, https://doi.org/10.5194/acp-22-15071-2022, 2022.

915 Uno, I., Wang, Z., Itahashi, S., Yumimoto, K., Yamamura, Y., Yoshino, A., Takami, A., Hayasaki, M., and Kim, B.-G.:
916 Paradigm shift in aerosol chemical composition over regions downwind of China, Sci. Rep., 10, 6450,
917 https://doi.org/10.1038/s41598-020-63592-6, 2020.
918 Wang, M., Kong, W., Marten, R., He, X.-C., Chen, D., Pfeifer, J., Heitto, A., Kontkanen, J., Dada, L., Kürten, A., Yli-Juuti,
919 T., Manninen, H. E., Amanatidis, S., Amorim, A., Baalbaki, R., Baccarini, A., Bell, D. M., Bertozzi, B., Bräkling, S., Brilke,
920 S., Murillo, L. C., Chiu, R., Chu, B., De Menezes, L.-P., Duplissy, J., Finkenzeller, H., Carracedo, L. G., Granzin, M., Guida,
921 R., Hansel, A., Hofbauer, V., Krechmer, J., Lehtipalo, K., Lamkaddam, H., Lampimäki, M., Lee, C. P., Makhmutov, V., Marie,
922 G., Mathot, S., Mauldin, R. L., Mentler, B., Müller, T., Onnela, A., Partoll, E., Petäjä, T., Philippov, M., Pospisilova, V.,
923 Ranjithkumar, A., Rissanen, M., Rörup, B., Scholz, W., Shen, J., Simon, M., Sipilä, M., Steiner, G., Stolzenburg, D., Tham,
924 Y. J., Tomé, A., Wagner, A. C., Wang, D. S., Wang, Y., Weber, S. K., Winkler, P. M., Wlasits, P. J., Wu, Y., Xiao, M., Ye,
925 Q., Zauner-Wieczorek, M., Zhou, X., Volkamer, R., Riipinen, I., Dommen, J., Curtius, J., Baltensperger, U., Kulmala, M.,
926 Worsnop, D. R., Kirkby, J., Seinfeld, J. H., El-Haddad, I., Flagan, R. C., and Donahue, N. M.: Rapid growth of new
927 atmospheric particles by nitric acid and ammonia condensation, Nature, 581, 184–189, https://doi.org/10.1038/s41586-020-
928 2270-4, 2020.
929 Wang, M., Xiao, M., Bertozzi, B., Marie, G., Rörup, B., Schulze, B., Bardakov, R., He, X.-C., Shen, J., Scholz, W., Marten,
930 R., Dada, L., Baalbaki, R., Lopez, B., Lamkaddam, H., Manninen, H. E., Amorim, A., Ataei, F., Bogert, P., Brasseur, Z.,
931 Caudillo, L., De Menezes, L.-P., Duplissy, J., Ekman, A. M. L., Finkenzeller, H., Carracedo, L. G., Granzin, M., Guida, R.,
932 Heinritzi, M., Hofbauer, V., Höhler, K., Korhonen, K., Krechmer, J. E., Kürten, A., Lehtipalo, K., Mahfouz, N. G. A.,
933 Makhmutov, V., Massabò, D., Mathot, S., Mauldin, R. L., Mentler, B., Müller, T., Onnela, A., Petäjä, T., Philippov, M.,
934 Piedehierro, A. A., Pozzer, A., Ranjithkumar, A., Schervish, M., Schobesberger, S., Simon, M., Stozhkov, Y., Tomé, A., Umo,
935 N. S., Vogel, F., Wagner, R., Wang, D. S., Weber, S. K., Welti, A., Wu, Y., Zauner-Wieczorek, M., Sipilä, M., Winkler, P.
936 M., Hansel, A., Baltensperger, U., Kulmala, M., Flagan, R. C., Curtius, J., Riipinen, I., Gordon, H., Lelieveld, J., El-Haddad,
937 I., Volkamer, R., Worsnop, D. R., Christoudias, T., Kirkby, J., Möhler, O., and Donahue, N. M.: Synergistic HNO3–H2SO4–
938 NH3 upper tropospheric particle formation, Nature, 605, 483–489, https://doi.org/10.1038/s41586-022-04605-4, 2022.
939 Wang, S., Peng, Y., Zhang, Q., Wang, W., and Wang, Q.: Mechanistic understanding of rapid H2SO4-HNO3-NH3 nucleation
940 in the upper troposphere, Sci. Total Environ., 883, 163477, https://doi.org/10.1016/j.scitotenv.2023.163477, 2023.
941 Wang, Z. B., Hu, M., Yue, D. L., Zheng, J., Zhang, R. Y., Wiedensohler, A., Wu, Z. J., Nieminen, T., and Boy, M.: Evaluation
942 on the role of sulfuric acid in the mechanisms of new particle formation for Beijing case, Atmospheric Chem. Phys., 11, 12663–
943 12671, https://doi.org/10.5194/acp-11-12663-2011, 2011.
944 Weber, R., Marti, J., McMurry, P., Eisele, F., Tanner, D., and Jefferson, A.: Measured atmospheric new particle formation
945 rates: Implications for nucleation mechanisms, Chem. Eng. Commun., 151, 53–64,
946 https://doi.org/10.1080/00986449608936541, 1996.

Xu, W., Gomez-Hernandez, M., Guo, S., Secrest, J., Marrero-Ortiz, W., Zhang, A. L., and Zhang, R.: Acid-Catalyzed Reactions of Epoxides for Atmospheric Nanoparticle Growth, J. Am. Chem. Soc., 136, 15477–15480, https://doi.org/10.1021/ja508989a, 2014.

Yan, C., Yin, R., Lu, Y., Dada, L., Yang, D., Fu, Y., Kontkanen, J., Deng, C., Garmash, O., Ruan, J., Baalbaki, R., Schervish, M., Cai, R., Bloss, M., Chan, T., Chen, T., Chen, Q., Chen, X., Chen, Y., Chu, B., Dällenbach, K., Foreback, B., He, X., Heikkinen, L., Jokinen, T., Junninen, H., Kangasluoma, J., Kokkonen, T., Kurppa, M., Lehtipalo, K., Li, H., Li, H., Li, X., Liu, Y., Ma, Q., Paasonen, P., Rantala, P., Pileci, R. E., Rusanen, A., Sarnela, N., Simonen, P., Wang, S., Wang, W., Wang, Y., Xue, M., Yang, G., Yao, L., Zhou, Y., Kujansuu, J., Petäjä, T., Nie, W., Ma, Y., Ge, M., He, H., Donahue, N. M., Worsnop, D. R., Kerminen, V.-M., Wang, L., Liu, Y., Zheng, J., Kulmala, M., Jiang, J., and Bianchi, F.: The Synergistic Role of Sulfuric Acid, Bases, and Oxidized Organics Governing New-Particle Formation in Beijing, Geophys. Res. Lett., 48, e2020GL091944, https://doi.org/10.1029/2020GL091944, 2021.

Yao, L., Garmash, O., Bianchi, F., Zheng, J., Yan, C., Kontkanen, J., Junninen, H., Mazon, S. B., Ehn, M., Paasonen, P., Sipilä, M., Wang, M., Wang, X., Xiao, S., Chen, H., Lu, Y., Zhang, B., Wang, D., Fu, Q., Geng, F., Li, L., Wang, H., Qiao, L., Yang, X., Chen, J., Kerminen, V.-M., Petäjä, T., Worsnop, D. R., Kulmala, M., and Wang, L.: Atmospheric new particle formation from sulfuric acid and amines in a Chinese megacity, Science, 361, 278–281, https://doi.org/10.1126/science.aao4839, 2018.

Yli-Juuti, T., Riipinen, I., Aalto, P. P., Nieminen, T., Maenhaut, W., Janssens, I. A., Claeys, M., Salma, I., Ocskay, R., Hoffer, A., Imre, K., and Kulmala, M.: Characteristics of new particle formation events and cluster ions at K-puszta, Hungary, 2009.

Yu, F., Nadykto, A. B., Herb, J., Luo, G., Nazarenko, K. M., and Uvarova, L. A.: H_2SO_4–H_2O–NH_3 ternary ion-mediated nucleation (TIMN): kinetic-based model and comparison with CLOUD measurements, Atmospheric Chem. Phys., 18, 17451–17474, https://doi.org/10.5194/acp-18-17451-2018, 2018.

Zaidan, M. A., Haapasilta, V., Relan, R., Paasonen, P., Kerminen, V.-M., Junninen, H., Kulmala, M., and Foster, A. S.: Exploring non-linear associations between atmospheric new-particle formation and ambient variables: a mutual information approach, Atmospheric Chem. Phys., 18, 12699–12714, https://doi.org/10.5194/acp-18-12699-2018, 2018.

Zhang, Y., McMurry, P. H., Yu, F., and Jacobson, M. Z.: A comparative study of nucleation parameterizations: 1. Examination and evaluation of the formulations, J. Geophys. Res. Atmospheres, 115, https://doi.org/10.1029/2010JD014150, 2010.

Zhao, B., Fast, J., Shrivastava, M., Donahue, N. M., Gao, Y., Shilling, J. E., Liu, Y., Zaveri, R. A., Gaudet, B., Wang, S., Wang, J., Li, Z., and Fan, J.: Formation Process of Particles and Cloud Condensation Nuclei Over the Amazon Rainforest: The Role of Local and Remote New-Particle Formation, Geophys. Res. Lett., 49, e2022GL100940, https://doi.org/10.1029/2022GL100940, 2022.

Zhou, Y., Hakala, S., Yan, C., Gao, Y., Yao, X., Chu, B., Chan, T., Kangasluoma, J., Gani, S., Kontkanen, J., Paasonen, P., Liu, Y., Petäjä, T., Kulmala, M., and Dada, L.: Measurement report: New particle formation characteristics at an urban and a mountain station in northern China, Atmospheric Chem. Phys., 21, 17885–17906, https://doi.org/10.5194/acp-21-17885-2021, 2021.

Figure 1. Map of measurement locations included in this study. The number markings indicate the exact locations of the measurements. Created using a template from Canva (www.canva.com)

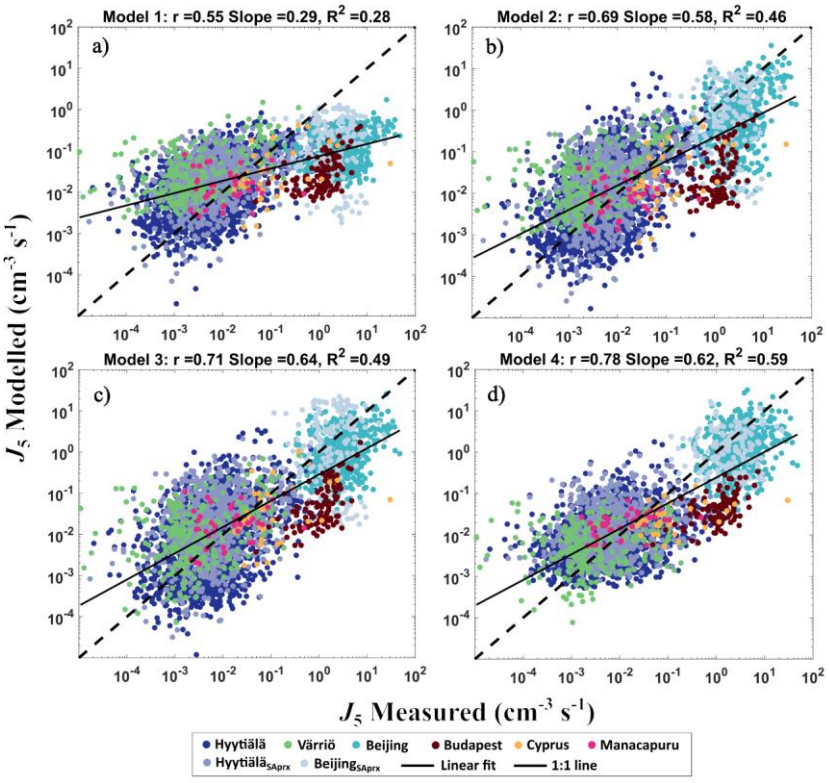

Figure 2. Modelled and measured J_5 scatterplots in logscale from four models using the testing dataset containing data from all sites in hourly time resolution. Each color represents the data from one measurement site, including datasets with H_2SO_4 proxy data from Hyytiälä and Beijing. The straight line showed the robust linear fit between the logscale modelled and the measure J_5 values, and the dashed line represented the 1:1 line. The correlation coefficient *r*, slope of linear fit, and the coefficient of determination R^2 are shown in the title of each subplot.

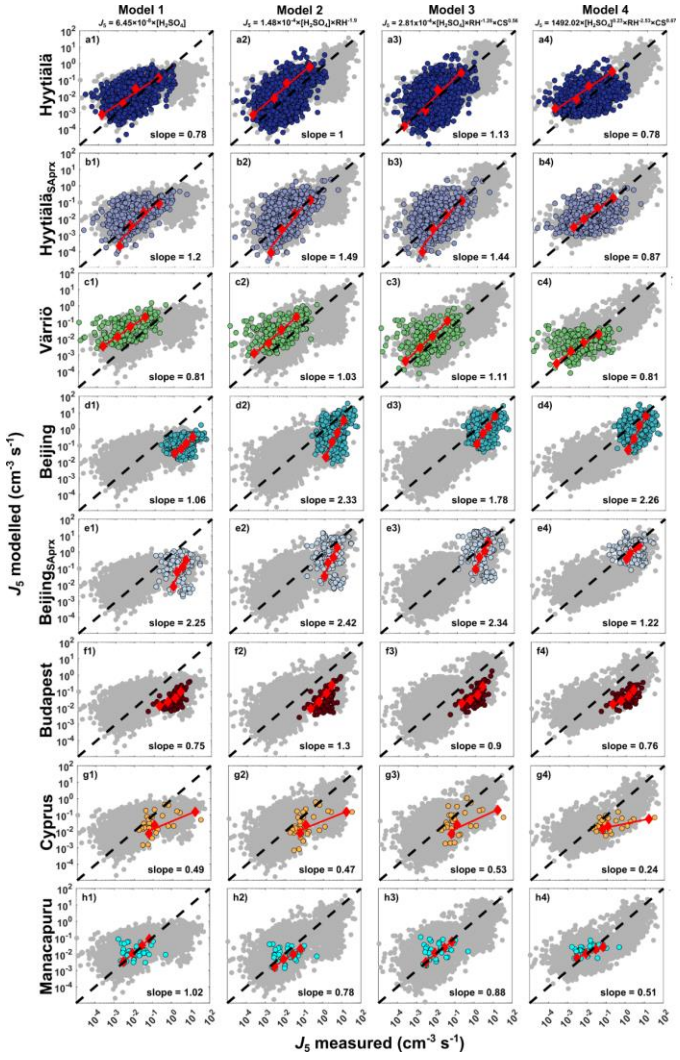

992

993 Figure 3. Modelled and measured J_5 scatterplots in logscale from four models using the testing dataset containing
994 data from all sites in hourly time resolution. The labels on the left side of the y-axis are the site names. The

995 subscribed label "SAprx" indicates that the input H_2SO_4 concentrations was from H_2SO_4 proxies. The light grey
996 scatters are all data points from the testing dataset, the colored scatters on top of them indicate the results from the
997 corresponding measurement site. The red diamonds are the binned daily medians to show the temporal aggregation
998 of the model performances on daily scale data. Overall, on a daily scale presents excellent performances on model
999 4 for boreal forest environment (a4, b4 and c4), polluted cities (d4, e4) and organic vapor dominated high humidity
1000 region (h1-h3). The red solid lines represent the linear fit on the binned hourly medians. The dashed line is the 1:1
1001 line.

1002

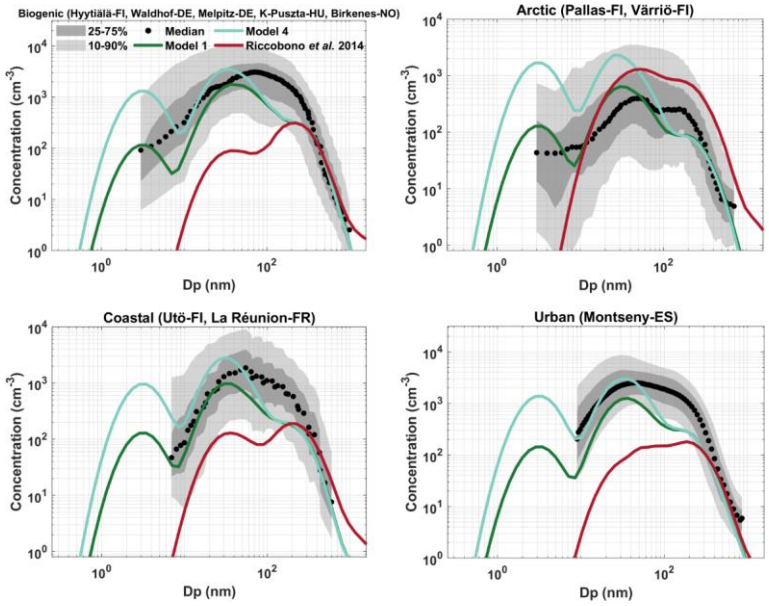

1003 Figure 4. Environment-specific TM5-MP simulated particle number size distribution from 2018 in annual medians.
1004 Biogenic sites include rural and rural regional background environments (Hyytiälä, Waldhof, Melpitz, K-Puszta
1005 and Birkenes); Coastal sites cover islands on the Baltic Sea and on the Indian Ocean in the southern hemisphere
1006 close to Madagascar (Utö and La Réunion); Arctic sites are two Finnish sites both situate within the Arctic Circle
1007 (Pallas and Värriö); Urban site is represented by a Spanish city Montseny.
1008
1009
1010
1011

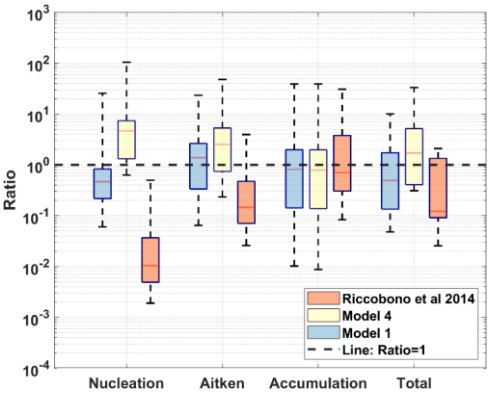

Figure 5. Ratio of simulated and measured particle number concentrations from the 14 global sites from TM5-MP simulations under three nucleation settings (Riccobono, model 1, and model 4) resulting in three particle modes (nucleation, Aitken, accumulation) in 2018 annual medians. The black line represents "ratio = 1" as a reference line. The "Total" represents the overall ratio between the simulation and the measurement particle number concentrations from all modes.

Table 1. Number of data points from each measurement site. The numbers in column "Total" account for the data points from six-site combined dataset utilized in model training and testing. The training set contains 75% of the total training data points, and 25% for testing set.

Sites	Hyytiälä	Beijing	Värriö	Budapest	Cyprus	Manacapuru	$\text{Hyytiälä}_{\text{proxy}}$	$\text{Beijing}_{\text{proxy}}$	Total
Training	5003	1342	728	367	140	140	-	-	7720
Testing	1642	501	248	109	34	40	797	164	3535

Table 2. Coefficient values (k_x, k_{RH}, k_{CS}, k_{SA}) retrieved from parameterization using training dataset. The term *SSe* represents the sum of squared error of each model. The units of k_x (x = 1, 2, 3, 4) vary as the functional form of model changes, while k_{RH}, k_{CS}, k_{SA} do not contain units. Since RH is counted using percentage (%), a dimensionless number, the scaling coefficients k0 count mainly the units from H_2SO_4 concentrations and CS. As such, we must ensure that the RH input is in percentage.

Models	Functional forms	k_x	k_{RH}	k_{CS}	k_{SA}	*SSe*
1	$k_1 \times [H_2SO_4]$	6.45E−8 (s^{-1})				2.78E+03
2	$k_2 \times [H_2SO_4] \times RH^{k_{RH}}$	1.48E−4 (s^{-1})	−1.9			5.16E+03
3	$k_3 \times [H_2SO_4] \times RH^{k_{RH}} \times CS^{k_{CS}}$	2.81E−4 ($[s^{-1}]^{0.45}$)	−1.28	0.56		5.18E+03
4	$k_4 \times [H_2SO_4]^{k_{SA}} \times RH^{k_{RH}} \times CS^{k_{CS}}$	1492.02 ($[cm^{-3}]^{0.78} \times [s^{-1}]^{0.33}$)	−2.53	0.67	0.23	3.36E+03

Table 3. Summary of overall and site-specific correlation coefficients (r) four models using the testing dataset. The numbers in brackets under the site names represent the count for data points.

		Slopes and *r* (robust linear fit), logscale								
	Models	Hyytiälä (1642)	Beijing (501)	Värriö (248)	Budapest (109)	Cyprus (34)	Manacapuru (40)	$\text{Hyytiälä}_{\text{SA}}$ (797)	$\text{Beijing}_{\text{SA}}$ (164)	Overall
Slope	1	0.43	0.33	0.32	0.58	0.35	0.04	0.34	0.07	0.30
	2	0.62	0.57	0.40	0.66	0.48	0.15	0.57	0.23	0.58
	3	0.48	0.43	0.32	0.85	0.37	0.18	0.42	0.12	0.64
	4	0.25	0.28	0.12	0.48	0.17	0.24	0.28	0.12	0.62
r	1	0.43	0.30	0.44	0.54	0.42	0.04	0.41	0.004	0.55
	2	0.47	0.32	0.47	0.46	0.49	0.19	0.48	0.07	0.69
	3	0.37	0.30	0.35	0.61	0.38	0.21	0.36	0.02	0.71
	4	0.31	0.22	0.18	0.51	0.37	0.46	0.33	0.09	0.78